AD-A161 298 THE INFLUENCE OF FLUID MECHANICS ON THE BEHAVIOR OF GAS-BLOWN SPARK GAP S..(U) TEXAS TECH UNIV LUBBOCK DEPT OF MECHANICAL ENGINEERING H J CARPER ET AL. 29 MAR 85 1/1

UNCLASSIFIED AFOSR-TR-85-0903 AFOSR-82-0327 F/G 9/1 NL

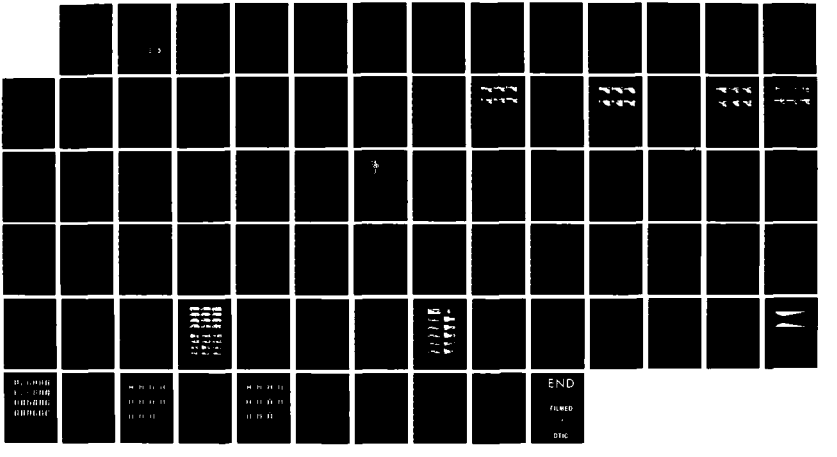

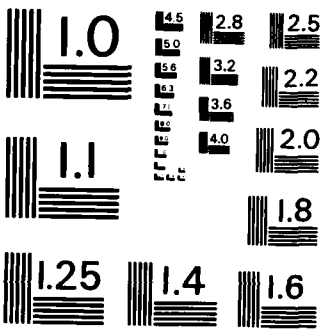

MICROCOPY RESOLUTION TEST CHART
NATIONAL BUREAU OF STANDARDS-1963-A

FINAL REPORT

on

THE INFLUENCE OF FLUID MECHANICS ON THE BEHAVIOR OF GAS-BLOWN SPARK GAP SWITCHES

March 29, 1985

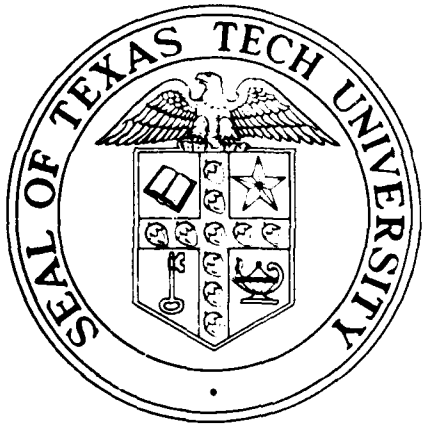

Air Force Office of Scientific Research
Grant No. AFOSR-82-0327

DEPARTMENT OF MECHANICAL ENGINEERING
TEXAS TECH UNIVERSITY

Lubbock, Texas 79409

Unclassified

SECURITY CLASSIFICATION OF THIS PAGE

REPORT DOCUMENTATION PAGE

1a. REPORT SECURITY CLASSIFICATION: Unclassified	1b. RESTRICTIVE MARKINGS
2a. SECURITY CLASSIFICATION AUTHORITY	3. DISTRIBUTION/AVAILABILITY OF REPORT: Distribution unlimited
2b. DECLASSIFICATION/DOWNGRADING SCHEDULE	
4. PERFORMING ORGANIZATION REPORT NUMBER(S)	5. MONITORING ORGANIZATION REPORT NUMBER(S): AFO[illegible] 3
6a. NAME OF PERFORMING ORGANIZATION: Dept. of Mechanical Engineering, Texas Tech University; 6b. OFFICE SYMBOL (If applicable)	7a. NAME OF MONITORING ORGANIZATION: AFOSR/NP
6c. ADDRESS (City, State and ZIP Code): Lubbock, Texas 79409	7b. ADDRESS (City, State and ZIP Code): Bolling AFB D.C. 20332-6448
8a. NAME OF FUNDING/SPONSORING ORGANIZATION: AFOSR; 8b. OFFICE SYMBOL (If applicable): NP	9. PROCUREMENT INSTRUMENT IDENTIFICATION NUMBER: Grant No. AFOSR-82-0327
8c. ADDRESS (City, State and ZIP Code): Bolling AFB D.C. 20332-6448	10. SOURCE OF FUNDING NOS.

PROGRAM ELEMENT NO.	PROJECT NO.	TASK NO.	WORK UNIT NO.
61102F		2301/A7	

11. TITLE (Include Security Classification): The Influence of Fluid Mechanics on the Behavior of Gas-Blown Spark Gap Switches

12. PERSONAL AUTHOR(S): Carper, Herbert Jackson, Jr. and Maxwell, Timothy T.

13a. TYPE OF REPORT	13b. TIME COVERED	14. DATE OF REPORT (Yr., Mo., Day)	15. PAGE COUNT
Final Scientific	FROM 82/9/30 TO 85/1/31	85/3/29	72

16. SUPPLEMENTARY NOTATION

17 COSATI CODES		
FIELD	GROUP	SUB. GR.

18. SUBJECT TERMS (Continue on reverse if necessary and identify by block number): Pulsed Power; Switching; Spark Gaps

19. ABSTRACT (Continue on reverse if necessary and identify by block number)

A research facility was designed and constructed to conduct experiments to determine the influence of fluid mechanics on the performance of gas-blown spark gap switches. The effects of gas flow velocity, electrode divergence angle and hydrodynamic boundary layer development were investigated for laminar flow in a switch consisting of a pair of electrodes mounted in a diverging nozzle configuration. The results of the experiments show that for a given set of operating conditions, a threshold gap velocity exists, and increasing the velocity above this value results in no improvement in switch performance. This threshold velocity is exponentially dependent on the electrode divergence angle, an increase in the latter resulting in a lower threshold velocity. The threshold velocity was found to vary nonmonotonically with the degree of hydrodynamic boundary layer development at the point of minimum gap spacing, and for the conditions investigated there is an optimum hydrodynamic entry length that results in a minimum threshold velocity. The effects of turbulence were investigated briefly with the results showing an improvement in switch performance with turbulence. A numerical model was developed to predict the transient gas density distribution produced in the flow by the arc. The results of the model prediction are compared with interferograms obtained during the experiments.

20. DISTRIBUTION/AVAILABILITY OF ABSTRACT	21. ABSTRACT SECURITY CLASSIFICATION
UNCLASSIFIED/UNLIMITED ☒ SAME AS RPT. ☐ DTIC USERS ☐	Unclassified

22a. NAME OF RESPONSIBLE INDIVIDUAL	22b. TELEPHONE NUMBER (Include Area Code)	22c. OFFICE SYMBOL
Maj. Henry L. Pugh	(202)767-4908	NP

DD FORM 1473, 83 APR EDITION OF 1 JAN 73 IS OBSOLETE.

Unclassified

SECURITY CLASSIFICATION OF THIS PAGE

Final Report

on

THE INFLUENCE OF FLUID MECHANICS ON THE BEHAVIOR OF GAS-BLOWN SPARK GAP SWITCHES

March 29, 1985

Air Force Office of Scientific Research

Grant No. AFOSR-82-0327

DEPARTMENT OF MECHANICAL ENGINEERING

TEXAS TECH UNIVERSITY

Lubbock, Texas 79409

TABLE OF CONTENTS

I. RESEARCH OBJECTIVES

1. Background

The research work reported herein was undertaken in an effort to contribute to the understanding of the physics involved in the flushing and recovery of the dielectric strength of gas-blown spark gap switches in repetitive operation. In recent years there has been an emphasis on increasing the repetition rates of these switches, with a suggested goal of 10 kilopulses per second (kpps) or higher for heavy-duty operation involving kilovolt and kiloamp levels. This goal is to be compared with repetition rates achieved by current switch designs of only several kpps. The importance of both fluid mechanics and heat transfer processes on the rate of recovery of the dielectric strength is generally recognized, but due to a lack of understanding of these processes, switch design to achieve high repetition rates has been dominated largely by trial and error experimentation.

There are many fluid mechanics, heat transfer, and geometric effects on the flushing and recovery process to be considered. The obvious beneficial effects of the flushing process are the physical displacement of the hot gas, which results from an arc discharge, from the interelectrode region as well as the cooling of the electrodes. There is also a significant contribution to the recombination process and gas cooling due to the mixing of the hot gas with the cooler purging gas. The electrode shape as well as the hydrodynamic and thermal boundary layers on the electrode surfaces will also influence the recovery process. For example, the gas velocity

throughout the hydrodynamic boundary layers is lower than the free-stream velocity in the central region between the electrodes, thus the flushing of the hot gas near the electrode surfaces is retarded. Another important factor is that the gas flow through the switch may be laminar or turbulent, and it would be expected that the recovery process would be enhanced by turbulence due to more vigorous mixing of the hot gas with the cooler purging gas.

It is envisioned that through research efforts, procedures and predictive techniques, which would take into account the various effects mentioned above, can be developed and used in a rational switch design process. One approach would involve a numerical solution of the momentum and energy equations for the gas flow through a switch of arbitrary geometry. This model would require simulation of the arc discharge and would solve for the gas density distribution as a function of time and space during the post-arc period. An electrical breakdown model for nonuniform gas density fields, similar to the well known Paschen [1] relationship for uniform density fields, would be included, and this breakdown model would necessarily include the statistical nature of the breakdown process. With the voltage versus time curve being superimposed on the predicted gas density field, the probability of prefires could be evaluated.

With the above background in mind, the present program was undertaken as a first step toward developing a predictive model for use in the design of a switch of arbitrary geometry. The program included an experimental phase to provide data on the effects of selected fluid mechanics variables on switch performance and to provide guidance in the development of the model.

2. Experimental Objectives

The first objective of the experimental program was to design and construct a research facility for conducting the experiments. This research facility was to include interferometric capabilities for obtaining interferograms which would show the transient gas density distribution in the interelectrode region during repetitive operation of the switch. The interferograms were to be used for observing the general nature of the flushing process and for comparison with the density predictions of the numerical model. The facility was also to include the capability to measure the variation of switch voltage with time during repetitive operation of the switch.

The primary fluid mechanics variables chosen for investigation were gas flow rate and electrode divergence angle, the latter being a variable of the flow geometry. The effects of boundary layer development and turbulence were also to be investigated. Data were to be obtained and analyzed to provide insight into the effects of these variables on switch performance.

3. Flow Modeling Objectives

The objective of the flow modeling was to initiate the development of a flow model which would solve numerically the governing momentum and energy equations for three-dimensional, compressible, laminar flow of a gas between a pair of electrodes of arbitrary shape with the arc discharge being simulated by a release of concentrated energy into the flow. The initial scheme to be evaluated included the use of body-fitted coordinates and

moving grid techniques. A solution for the velocity field in the inter-electrode region was to be obtained for the two-dimensional switch geometry employed in the experiments. The arc energy release into the flow was to be introduced into the model, and a solution was to be obtained for the transient gas density field in the interelectrode region.

II. EXPERIMENTAL APPARATUS AND PROCEDURES

1. Research Facility

The research facility which was designed, constructed, and employed for the experiments is shown schematically in Figure 2.1. An untriggered, repetitive arc is produced between two electrodes, mounted in the electrode test section, by an R-C circuit connected to a 10 kW power supply with variable, no-load output voltage, E_o, of up to 20 kV d.c. The capacitor, C, which fixes the maximum energy per discharge, has a capacitance of 0.01 μf. The load resistor, R_L, limits the current conducted across the gap and has a resistance of 24.6 Ω. The charging resistor, R_c, along with the power supply voltage, establishes the charging rate of the capacitor and has a resistance of 100,500 Ω.

The voltage across the electrodes during operation of the switch was measured by using a Tektronix model P6015, 1000:1 high-voltage d.c. probe and a 2:1 voltage divider connected to a Data Translation, intelligent analog peripheral board mounted in an IBM CS-9000 computer. This data acquisition system can record voltage data at a rate of up to 40 kHz with 12 bit A/D conversion. Permanent storage for data is provided by 8-in. floppy disks. The data acquisition system is housed in a double-walled isolation screen room in order to shield it and other instrumentation from RF noise generated by the switch during operation. To avoid ground loops, the screen room and all grounds are connected to a central earth ground stake. The power supply of the data acquisition system is protected from line surges with a Gould model DT250R5 computer grade isolation transformer.

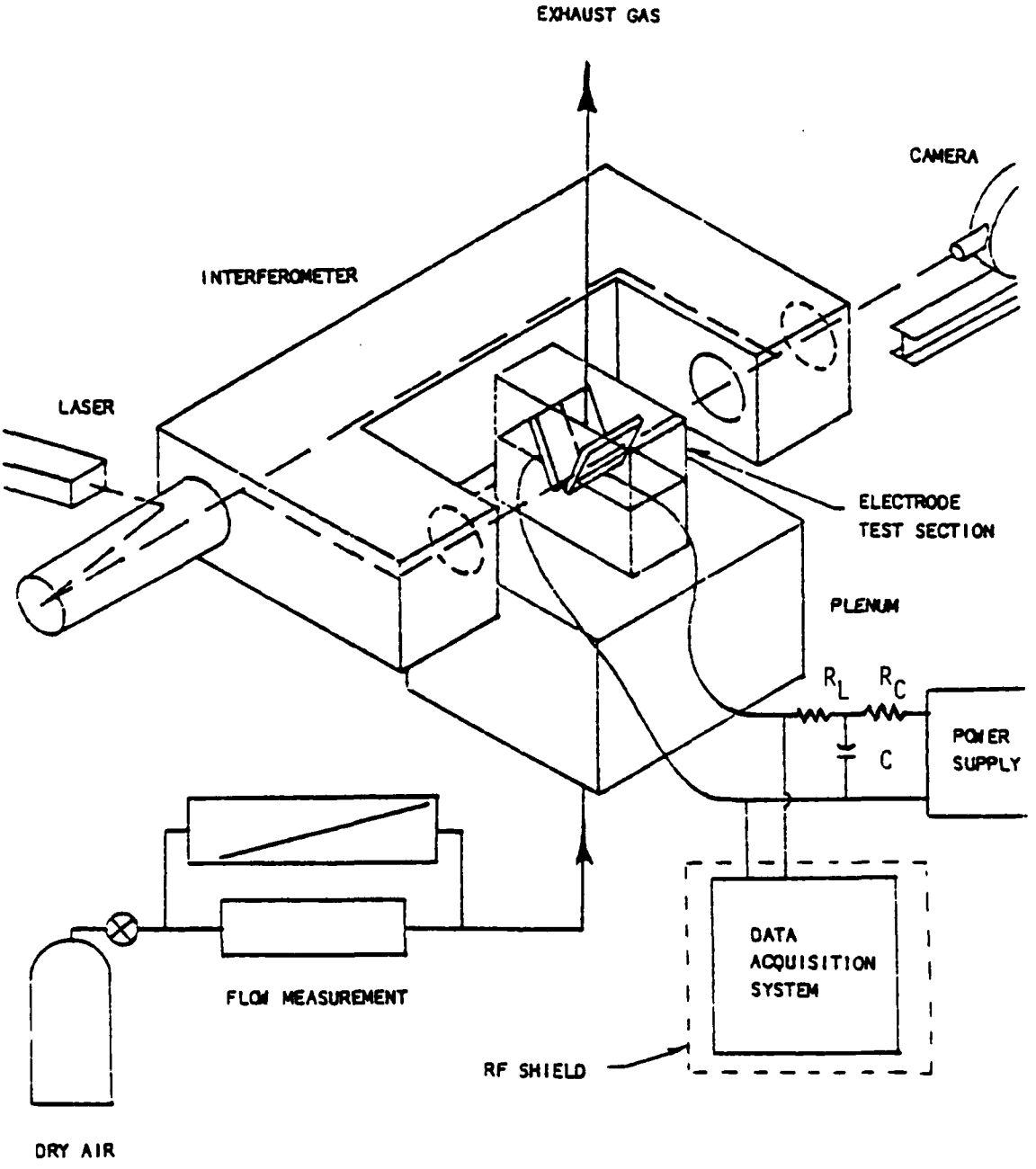

Figure 2.1 Gas-Blown Spark Gap Research Facility

The switch is purged by instrument grade, bottled dry air supplied to a plenum and is exhausted to the atmosphere after flowing through the electrode test section. Gas flow rate is measured through the use of a calibrated laminar flow element and manometers.

The electrode test section is located in the test section of a Mach-Zehnder interferometer. A 15 mW helium-neon laser is used for the light source of the interferometer, and interferograms showing gas density distribution in the interelectrode region can be obtained by using one of a variety of high-speed cameras mounted on an optical rail.

The configuration of the electrode test section is shown in detail in Figure 2.2. The basic geometry consists of a set of diverging electrodes housed in a wind tunnel. The electrodes are mounted in Lexan holders which form two opposing walls of the wind tunnel, and the other two sides of the wind tunnel are flat Plexiglas plates. The test section is designed for ease of adjustment of the minimum electrode separation distance (minimum gap spacing) and the angle of divergence to facilitate investigation of the effects of these two geometrical variables on switch performance. For all experiments conducted in the present study, the minimum gap spacing was set to 2.54 mm. The aspect ratio of the wind tunnel, based on this minimum gap spacing, was 40:1 resulting in a close approximation to two-dimensional flow in the test section.

For the bulk of the experiments, the electrodes used were thin strips of 304 stainless steel machined according to the design shown in Figure 2.3. All machined electrodes were made from the same sheet of steel. The electrodes are located at the lateral midplane of the test section, and are inserted in slots cut in the holders such that each electrode is flush with

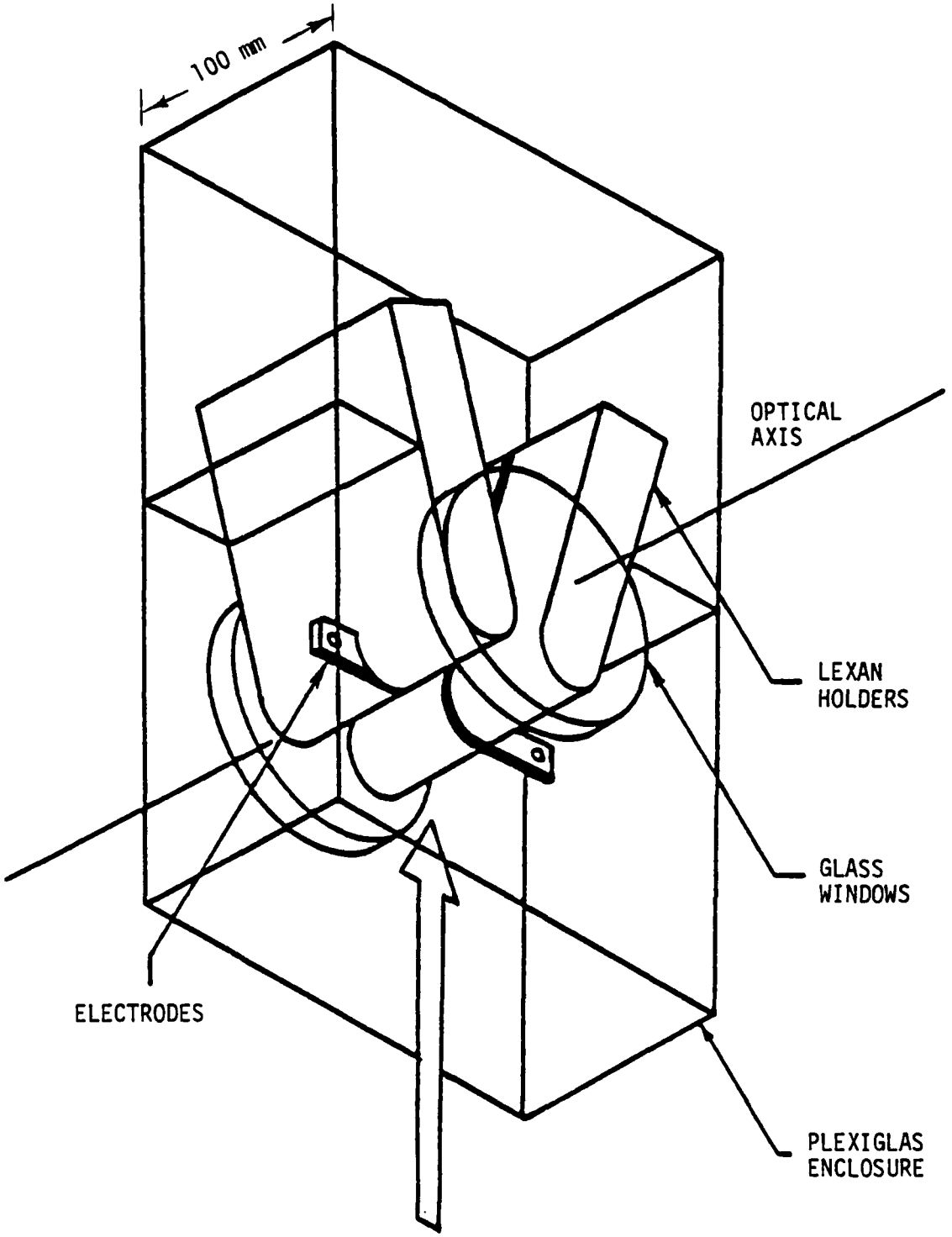

Figure 2.2 Electrode Test Section

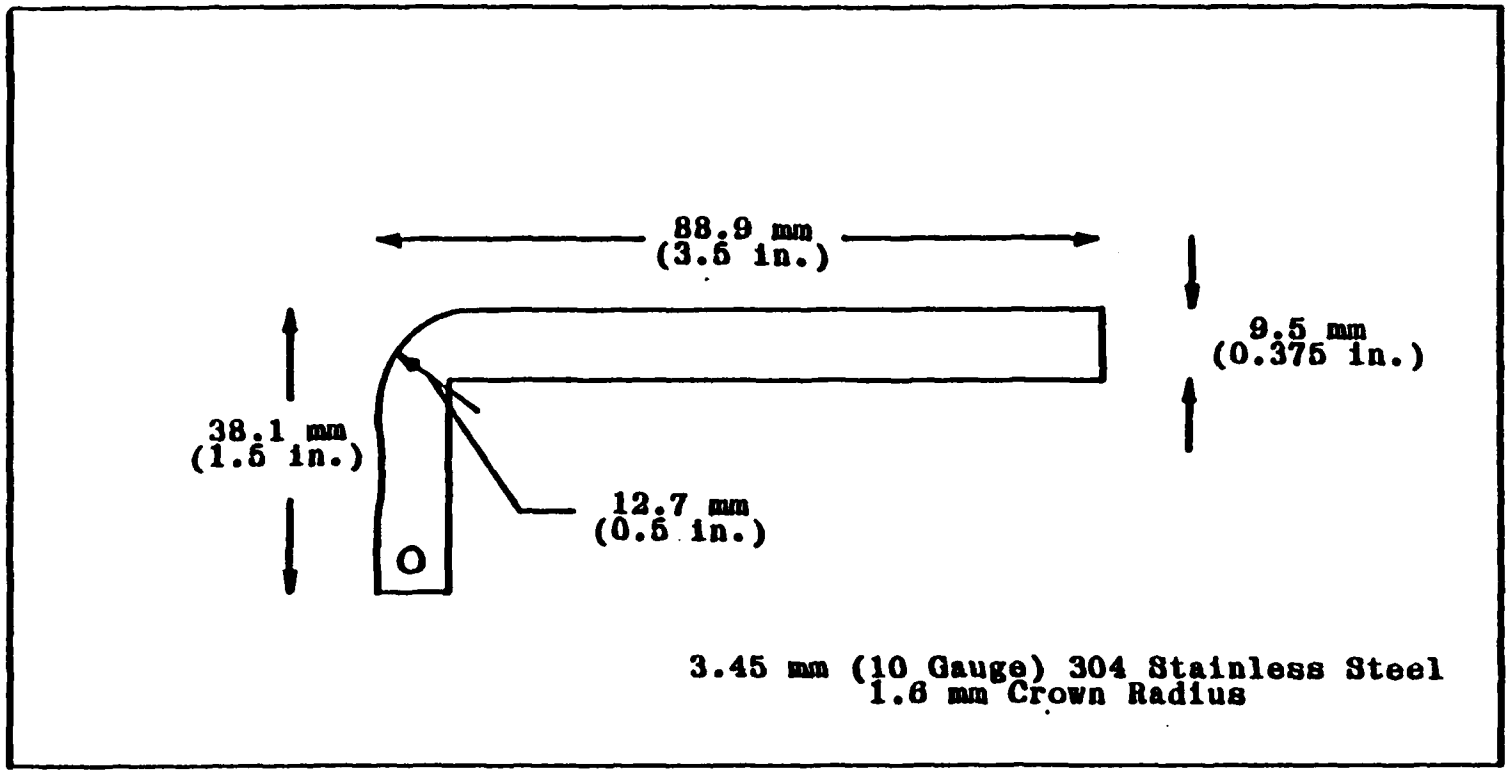

Figure 2.3 Electrode Design

the surface of its holder. Thin electrodes are used in order to confine the arc to the midplane where the camera is focused, and high-quality optical glass windows are installed in the Plexiglas sides of the wind tunnel on the optical axis to allow undistorted viewing of the arc and its effects on gas density with the interferometer. The leading edges of the electrode holders are machined with a radius equal to their half-width to provide smooth transition of the gas flow from the plenum to the interelectrode region, and the electrodes are machined with this same radius. To avoid arcs forming at the electrode-holder interfaces, the electrodes are also provided with a crown radius, approximately equal to their half-width, which extends over their entire length. To investigate the effects of a simpler electrode design, some experiments were conducted with 3.175-mm diameter, 308 stainless steel rods, bent to conform to the slot in the leading edges of the electrode holders.

To investigate the effects of hydrodynamic boundary layer development on switch performance, Plexiglas ducts of various lengths could be attached to the test section as shown in Figure 2.4. The entry length duct extended down into the plenum as shown in Figure 2.5.

2. Electrode Preparation and Installation

The machined electrodes were ultrasonically cleaned in a Freon TF bath for a period of 15 minutes after the machining process. They were then allowed to dry for 30 minutes before being uniformly sandblasted using 50-micron diameter aluminum oxide powder. During preliminary experiments it was found that this surface finish provided the most consistent switch performance when compared with machined, polished, or sandpapered finishes.

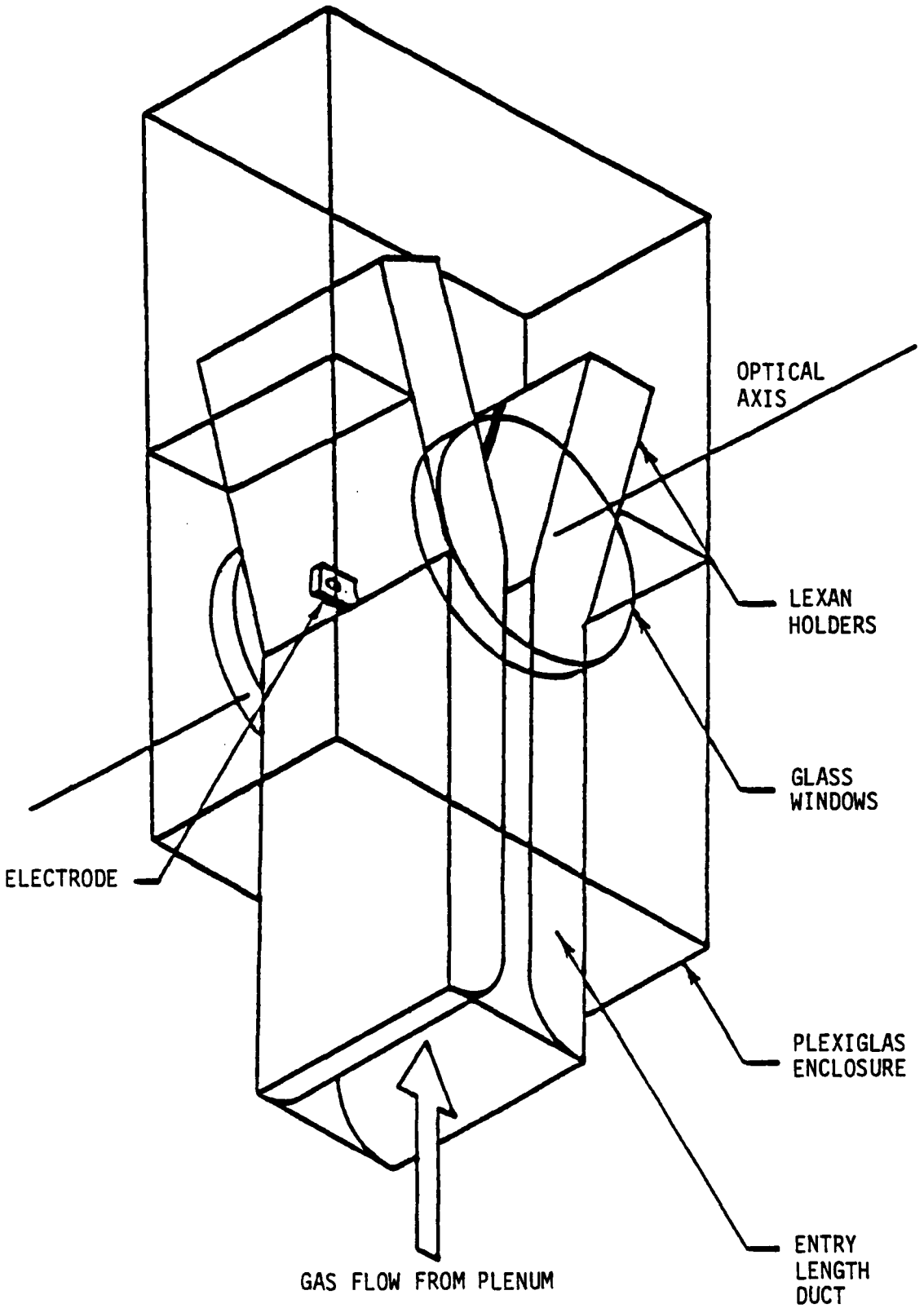

Figure 2.4 Electrode Test Section with Entry Length Duct

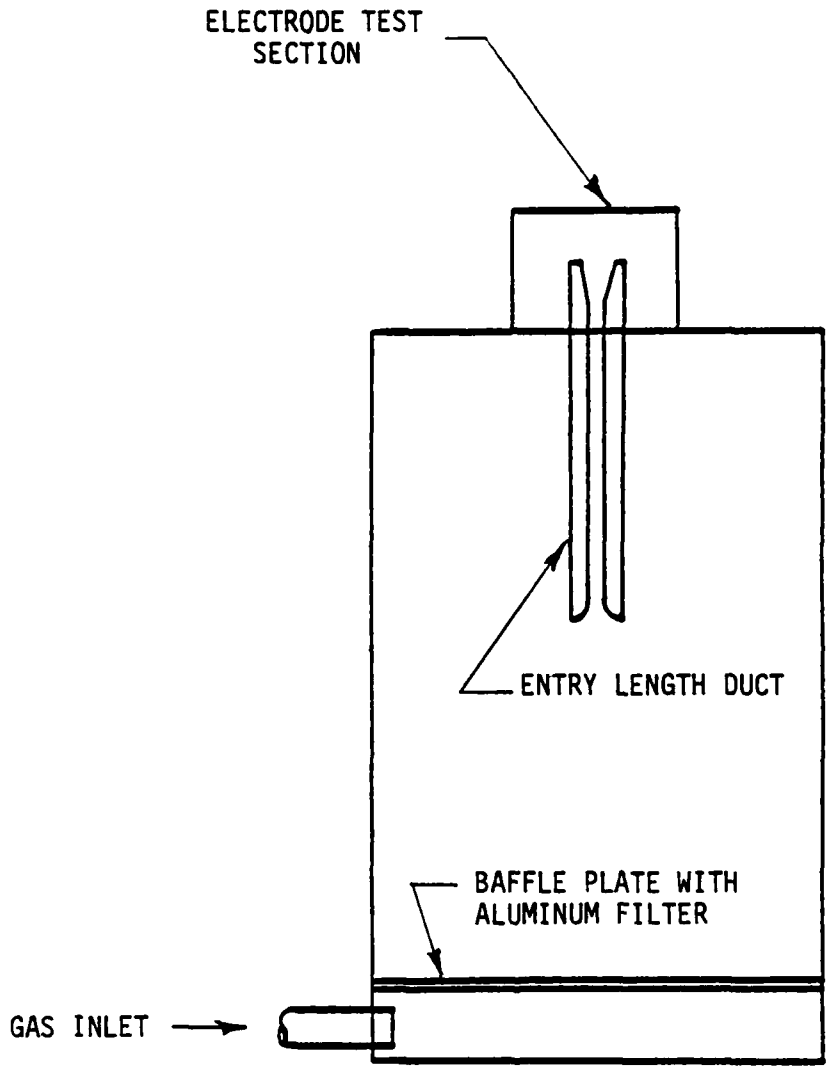

Figure 2.5 Sketch of Plenum with Entry Length Duct Installed

After sandblasting, the electrodes were stored in an airtight glass jar which was purged with dry air to minimize moisture adsorption. Prior to testing, the electrodes were once again ultrasonically cleaned in Freon TF for 15 minutes and allowed to dry for 30 minutes. The cleaned and dried electrodes were then inserted into the holders, and the holders were installed in the electrode test section. The desired electrode divergence angle was set using a machined wedge, and the minimum gap spacing was set to 2.54 mm by using a dowel pin gage.

3. General Operating Characteristics of the Switch and Selection of Operating Variable Ranges

Before the formal testing program was initiated, experiments were first conducted to determine the general operating characteristics of the switch and to select the ranges of the operating variables. With a minimum gap spacing of 2.54 mm, the static breakdown voltage was determined to be approximately 9 kV. The current wave form of a single arc displayed a pulse width of about 3 μs, with ringing out to about 10 μs, and a maximum current of about 150 amperes.

The gas flow rate through the switch is characterized herein by the average gap velocity, $\overline{U}$, which is the average velocity in the plane of minimum gap spacing. The maximum value of $\overline{U}$ was selected to be approximately 17 m/s. This maintained the time duration of the flushing process within the capabilities of the high-speed cameras used to obtain the interferograms. The maximum Reynolds number, based on the hydraulic diameter of the test section at minimum gap spacing was less than 5,000. The resulting flow in the electrode test section was laminar. As discussed later, turbulence was generated artificially to study its effect on switch performance.

The maximum value selected for the electrode divergence angle, θ, was chosen to be 10°. At angles greater than 10°, there is a high probability of hydrodynamic boundary layer separation which would result in backflow in the switch.

From the results of the preliminary experiments, the no-load charging voltage, E_o, for the formal testing program was chosen to be 14,400 volts. This resulted in a charging voltage under loaded conditions with the switch operating repetitively of 11,800 volts. The maximum charging voltage was limited since for certain conditions of electrode divergence angle and gas flow rate, using too high a voltage resulted in the formation of a continuous arc. In these cases, the charging rate was too high relative to the rate of recovery of the dielectric strength of the switch. With an E_o of 14,400 volts, and the switch operating normally, the nominal repetition rate was about 550 pulses per second.

4. Development of Switch Performance Criteria

In order to quantify switch performance, voltage data obtained with the data acquisition system during repetitive operation of the switch were analyzed by using software developed during the present program. The performance criteria were formulated from the results of experiments conducted prior to the initiation of the formal testing program. These preliminary experiments involved obtaining voltage data and interferograms simultaneously while the switch was operating repetitively with blowing. The interferograms were obtained by the infinite fringe method with a Fastax, 16-mm camera operating at speeds up to about 4,200 pictures per second. Through comparison of the voltage data with the interferograms, it was

possible to identify four distinctive switch breakdown events. These have been designated as 1) normal breakdown, 2) extended breakdown, 3) prefire, and 4) multiple low voltage prefire. An example of each of these events is presented in the four figures which follow. Each figure contains a partial sequence of interferograms with the corresponding voltage data presented in analog form below the interferograms. For all these examples, the average gap velocity, $\bar{U}$, is 4.1 m/s, and the electrode divergence angle, θ, is 10°. The gas flow direction is from left to right. The camera speed is approximately 4,000 pictures per second, resulting in an elapsed time of about 250 μs per frame and an exposure time of about 96 μs. The interferograms presented are not equally spaced in time, some having been removed from the continuous sequence to conserve space. The interferogram prints were made from positive film, and thus appear as negatives. That is, what would appear bright to the eye appears dark on the prints and vice versa.

Figure 2.6 presents a sequence of interferograms showing a normal breakdown and the resulting hot gas being flushed from the interelectrode region during simultaneous recharging of the capacitor. The voltage curve has been labeled a through f to correspond approximately to the events depicted by the interferograms. Interferogram (a) shows the normal discharge arc which formed at the minimum gap spacing and corresponds to the portion of the voltage curve labeled a, where the voltage dropped from about 9.5 kV to 2.5 kV. The hot gas resulting from the previous breakdown had already been blown downstream of the minimum gap region, and are seen as the white mass to the right in interferogram (a). This allowed the switch to regain its full pre-arc dielectric strength upstream before the occurrence of the normal discharge shown.

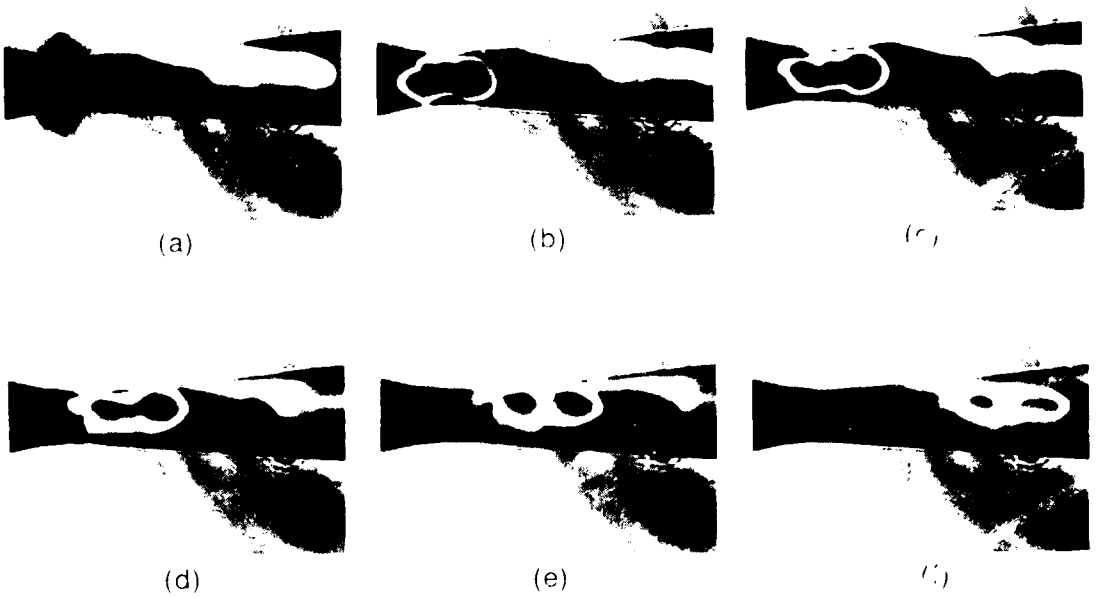

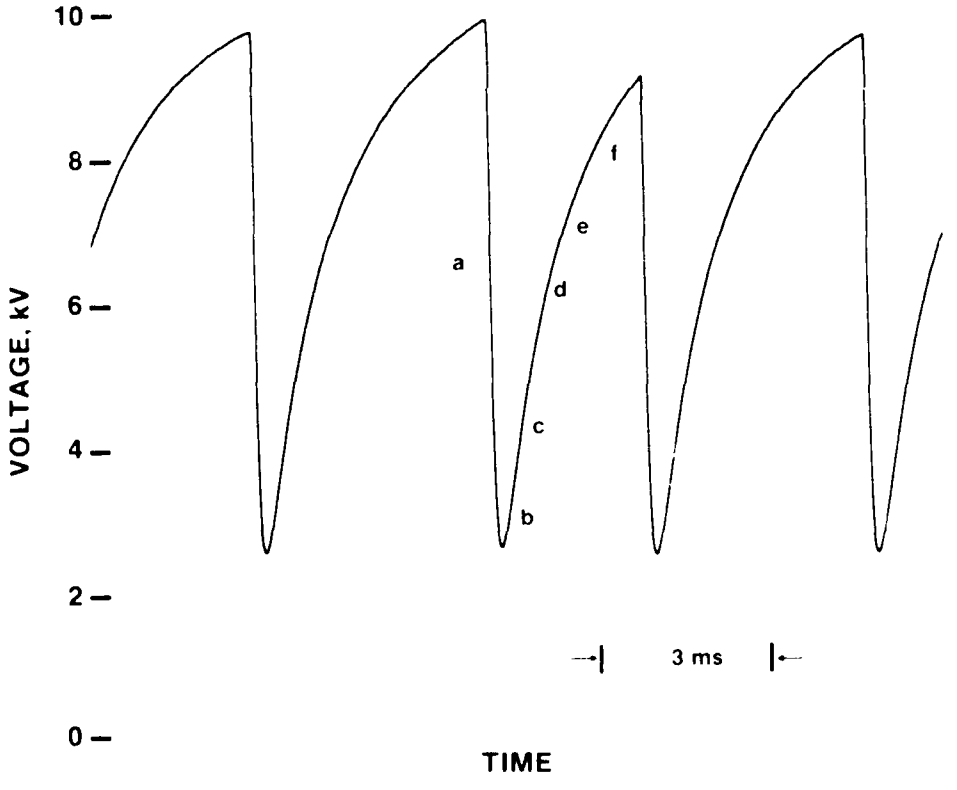

Figure 2.6 Example of a Normal Breakdown, $\bar{U}$ = 4.1 m/s, θ = 10°

It can be seen in interferogram (b) that initially the hot gas region is almost symmetrical about the point of discharge, having yet to be displaced by the blowing gas. At this point in time, the dielectric strength of the switch had been greatly reduced due to the decreased density of the heated gas and the increased electrode surface temperature. However, since a finite time is required to recharge the capacitor, time was allowed for the hot gas to be flushed out of the switch before the next discharge occurred (not shown in the interferograms). As can be seen in interferograms (c) through (f), the region of lower density gas was blown from the switch as the capacitor was recharging along the portion of the voltage curve labeled b through f.

Figure 2.7 presents an interferogram sequence containing an extended breakdown. Interferogram (a) shows the normal arc, which was followed immediately by another distinct arc, visible in interferogram (b). Interferograms (c) through (f) show the hot gas subsequently being flushed from the interelectrode region. The voltage curve has been labeled a through f, again indicating an approximate correspondence with the events depicted in the interferogram sequence. The normal breakdown shown in interferogram (a) corresponds to the voltage drop from approximately 10 kV to the point of the normal quench level, typically 2.5 kV. Interferogram (b), which shows the extended breakdown, corresponds to the section of the voltage curve labeled b, depicting a further voltage drop of approximately 1.0 kV before the arc finally quenched. This second arc occurred so rapidly after the first breakdown that there is no evidence of any attempted voltage recovery of the gap. The remaining interferograms, (c) through (f), show that after this extended breakdown, the switch returned to

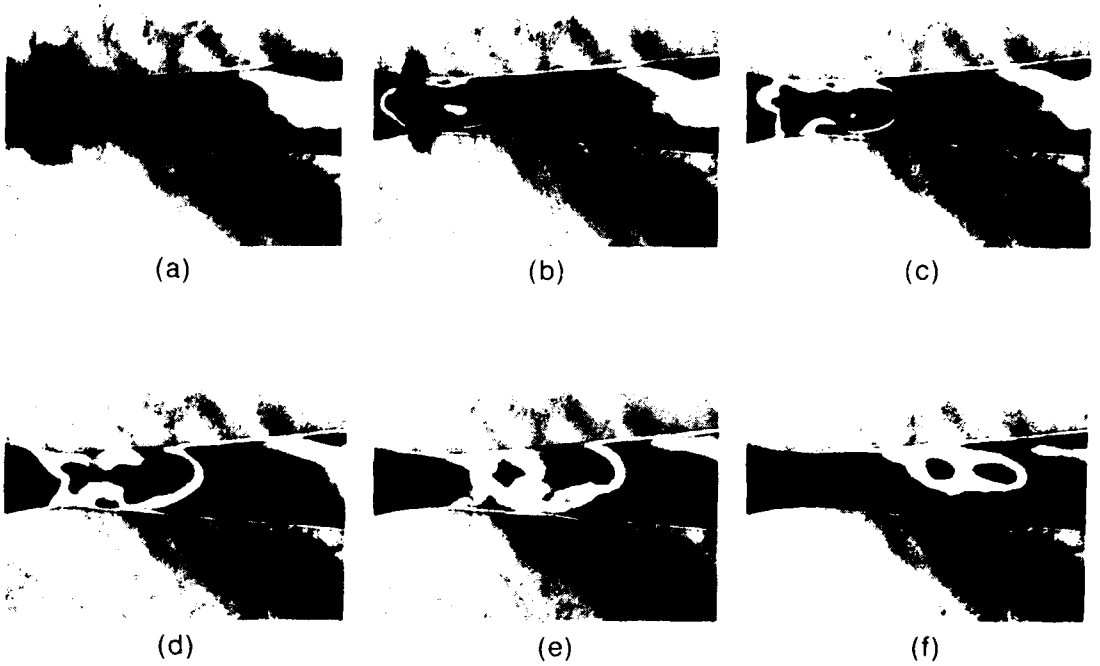

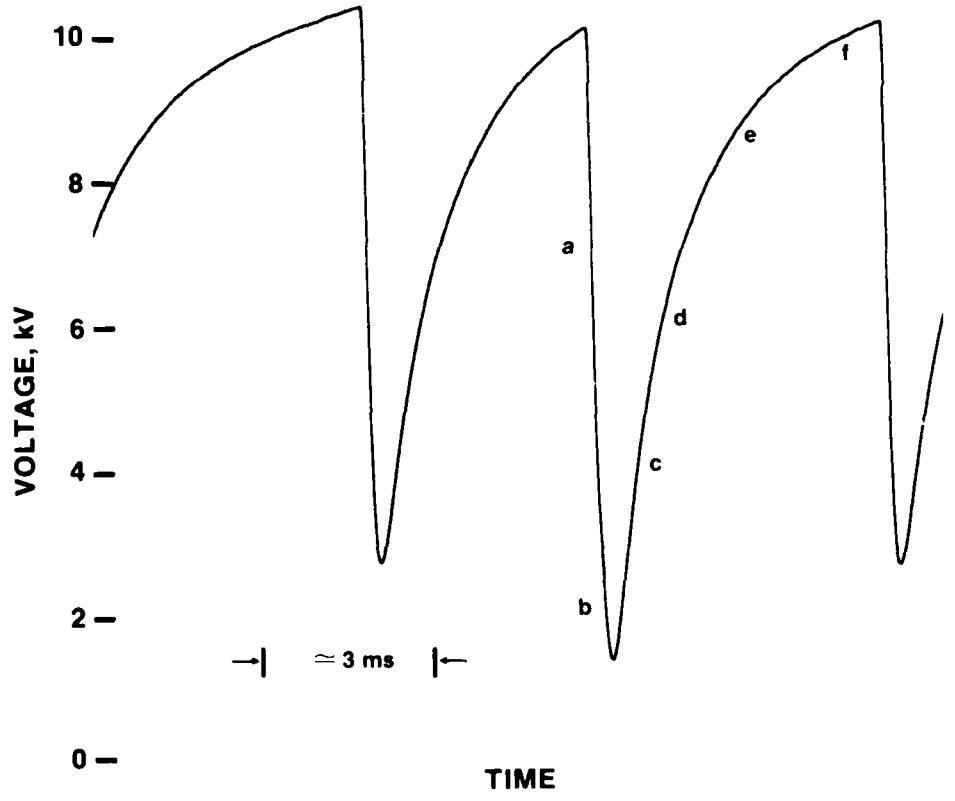

Figure 2.7 Example of an Extended Breakdown, $\overline{U}$ = 4.1 m/s, θ = 10°

its normal process of flushing during the simultaneous recharging of the capacitor indicated by the portion of the voltage curve labeled c through f.

Figure 2.8 presents a sequence of interferograms containing a typical prefire. A prefire is defined herein as a single discharge occurring downstream of the minimum gap spacing, through the hot gas resulting from a previous normal breakdown, at a voltage considered lower than normal. Interferogram (a) shows the hot gas region appearing immediately after a normal breakdown and corresponds to the portion of the voltage curve labeled a. Similarly, interferograms (b) through (d) show the hot gas being moved downstream by the flow, during which time the capacitor was being recharged corresponding to b through d on the voltage curve. Interferogram (e) captured the prefire, which occurred through the hot gas region located approximately 2.5 minimum gap spacings downstream of the point of the normal breakdown, and at a voltage noticeably less than that of the normal breakdown. Interferogram (f) shows an extended breakdown which materialized after the prefire.

Figure 2.9 presents a typical case of the multiple low voltage prefire. Interferogram (a) shows the arc of a normal discharge, and interferogram (b) shows the secondary arc created by an extended breakdown as discussed above. But rather than the arc quenching at this point, allowing the hot gas to be flushed from the switch, a series of low voltage discharges occurs, selected examples of which are presented in interferograms (c) and (d). The high-frequency nature of the event can be seen in the corresponding voltage curve. In the case of a multiple low voltage prefire, each arc in the sequence occurs at continually increasing distance downstream of the minimum gap spacing, until at some point the final arc

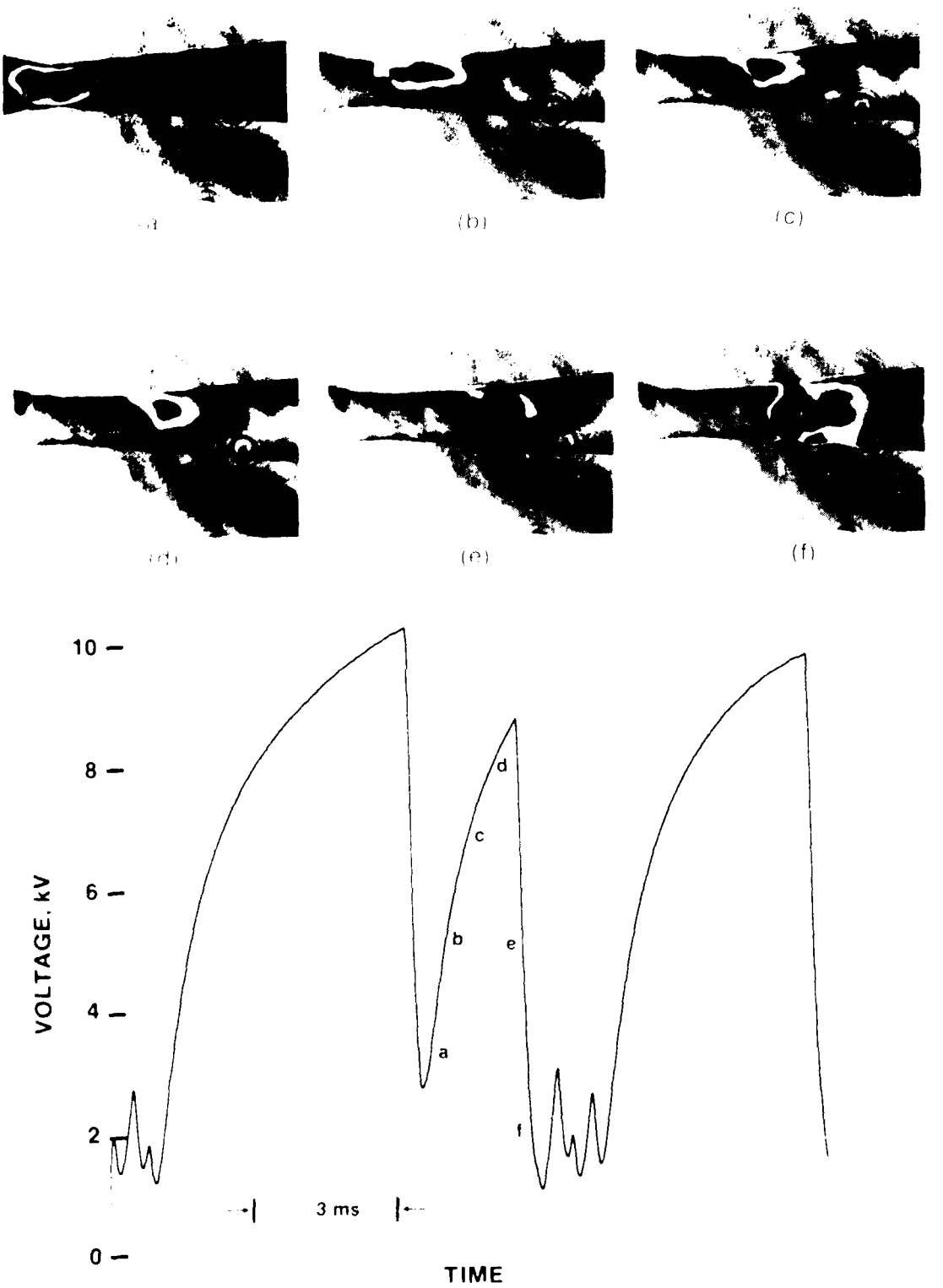

Figure 2.8 Example of a Prefire, $\bar{U}$ = 4.1 m/s, θ = 10°

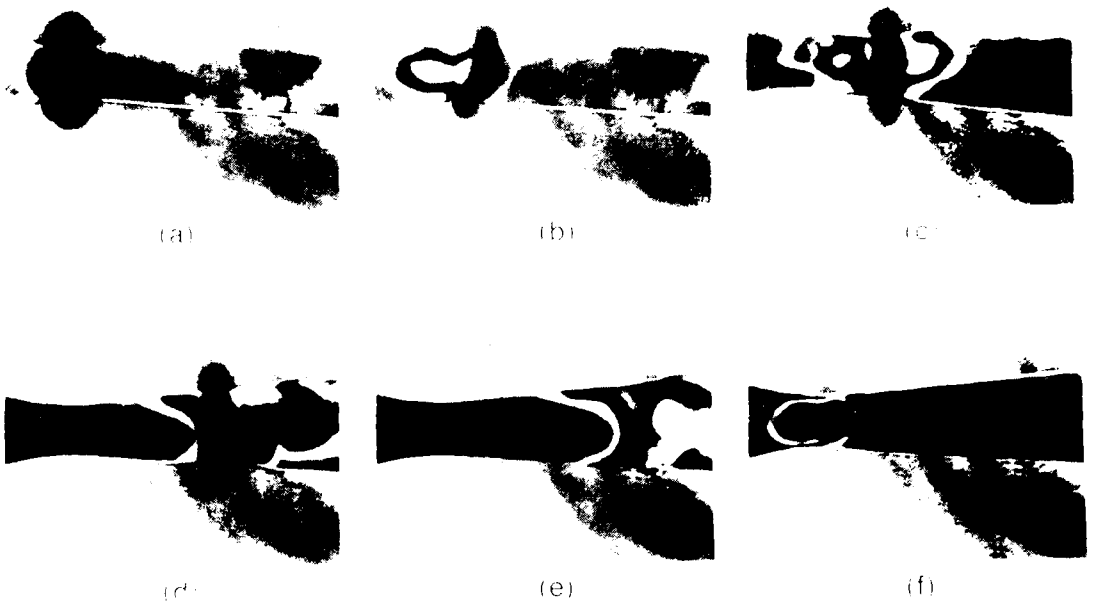

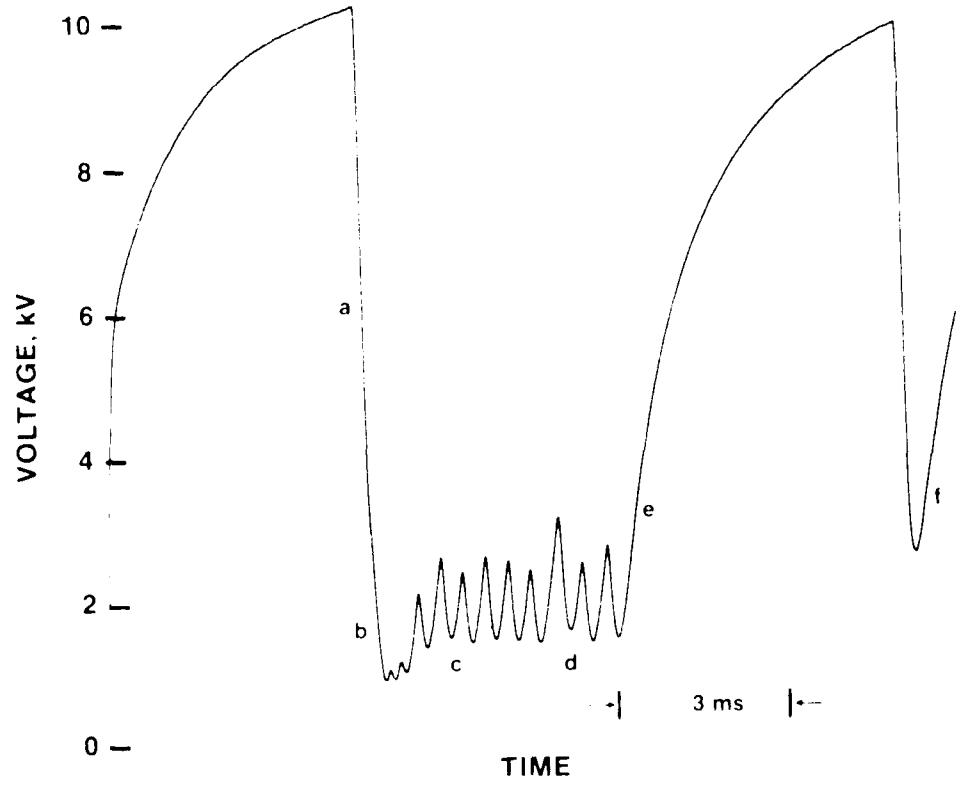

Figure 2.9 Example of a Multiple Low Voltage Prefire, V = 4.1 m/s, [illegible] = 10

quenches. Interferogram (e) shows the location of the hot gas region immediately following the last arc, ready to be flushed from the interelectrode region during the simultaneous recharging of the capacitor.

In all of the interferogram sequences obtained, the termination of a multiple low voltage prefire was followed by a normal breakdown. Furthermore, the breakdown voltage of this normal breakdown was generally of greater magnitude than the breakdown voltage normally associated with a discharge at the minimum gap spacing. It is theorized that while the multiple low voltage prefire is occurring downstream of the point of minimum gap spacing, the upstream end of each electrode is being cooled below its normal operating temperature. Thus, the amount of time for any retained thermal energy to be transferred to the cooler blowing gas is increased, due to the duration of the multiple low voltage prefire. The result is a higher than normal dielectric strength for the switch due to a decrease in temperature of the thermal boundary layer along each electrode.

Having determined the tendencies and characteristics of the normal breakdown, the extended breakdown, the prefire, and the multiple low voltage prefire, the following quantitative criteria were developed for use in the data reduction program.

The normal breakdown was defined as one having a breakdown voltage equal to or greater than 90 percent of the average static breakdown voltage recorded for each set of electrodes. To confirm that a breakdown had occurred, two consecutive voltage drops of 60 volts or more were required, immediately after the suspected breakdown voltage, to insure that the data reduction program ignored any slight data fluctuations due to noise, RF interference, A/D accuracy, etc. The prefire was defined as a breakdown

which occurred at a voltage less than 90 percent of the static breakdown voltage but greater than 110 percent of the average minimum quenching voltage for the data set. Although somewhat arbitrary, examination of data sets containing a wide variety of prefires and normal breakdowns, several linked directly with the interferograms obtained using the high-speed camera, indicated this was a reasonable definition.

An extended breakdown was considered to have occurred if the minimum quenching voltage after either a normal breakdown or a prefire was less than 90 percent of the average minimum quenching voltage of the entire data set, a value which typically varied by less than 200 volts.

A multiple low voltage prefire was considered to have occurred when a breakdown voltage less than the average minimum quenching voltage was encountered as the next event following an extended breakdown. Once initiated, a multiple low voltage prefire was not considered completed until a voltage of at least 90 percent of the static breakdown voltage, i.e., a normal breakdown, was reached.

5. Testing Procedure

For the formal testing program, the procedure described here was adopted. Prior to connecting each pair of electrodes to the R-C circuit, the no-load charging voltage was adjusted to 14,400 volts. This adjustment was necessary prior to each test since the ouput voltage of the power supply was found to vary substantially with line voltage, which at times varied throughout the day. A mechanical stop on the power supply voltage control was adjusted to obtain the desired no-load voltage. The electrodes were then connected, and several static breakdown measurements were

performed. Each static breakdown test consisted of slowly increasing the power supply voltage until a single breakdown occurred. These static breakdown voltages were then recorded and averaged.

After the gas flow rate had been established, a six-second repetitive operation test was conducted. This test consisted of two seconds of unmonitored operation followed by three seconds of data acquisition at 20,000 samples per second, followed by one second of unmonitored operation. As many as five such tests were conducted on each electrode pair, each test being designated by a sequential test number, N. A ten-minute period was allowed for the system to cool to its initial state before the next six-second test was conducted.

6. Data Analysis Techniques

Each three-second set of voltage data was analyzed by a computer code, which employed the previously discussed set of switch performance criteria, to determine all breakdown voltages, the mode of the breakdown voltages, the sequence of occurrence of the various events, and the average minimum quenching voltage. These data were stored on an output file for further analysis.

The test conditions were such that, in any three-second test, the switch operated with a preponderance of normal breakdowns, but with some prefires so that the effects of the various fluid mechanics variables on the probability of the occurrence of a prefire could be determined. The number of prefires occurring in any three-second test was relatively small, and due to the statistical nature of their occurrence considerable variation in performance from one electrode pair to another was sometimes

observed. For this reason, from two to five pairs of electrodes were tested at the same conditions. In the case of repeat tests, data sets for the same sequential test number, N, were combined and treated as one.

Each combined data set for a given N could be analyzed in various ways. A histogram including all breakdown voltages in the data set could be obtained, or the normal breakdowns could be extracted and a histogram of the normal breakdowns alone could be obtained. Histograms of the latter type are presented later in this report to show the effect of accumulated electrode operating time on switch performance. As will be seen, switch performance varies significantly with accumulated electrode operating time as a result of a varying electrode surface condition. To exclude this effect in the determination of the effects of gas flow velocity, electrode divergence angle, hydrodynamic boundary layer development, and turbulence on switch performance, only the data for N = 1, representing the first three seconds of data obtained with a new pair of electrodes, were analyzed.

Each combined data set for a given set of test conditions for N = 1 was then scanned to group the breakdowns into two-pulse "experiments." These experiments were defined such that the first pulse, or breakdown, had to be a normal breakdown whose breakdown voltage was within a given voltage of the average mode. The second pulse, which could be either another normal breakdown or a switch failure, was viewed as the result of the experiment. Analysis of the data in terms of these two-pulse experiments then provided a means of determining the probability of a failure following a normal breakdown.

Allowing an experiment to begin with a breakdown within a limited voltage range was effected as a compromise to make the initial breakdowns as identical as possible, while at the same time maximizing the total number of experiments in any one combined data set. The effects of three voltage ranges were investigated, ±50, ±100, and ±200 volts. These three ranges allowed for a variation of energy input of ±1, ±2.5, and ±5 percent, respectively, based on the difference in the squares of the average mode and the average minimum quenching voltage. The ±50 volt range severly limited the number of experiments admitted and was considered to be too small. The two remaining voltage ranges admitted nearly the same number of experiments and therefore a ±100 volt range was adopted.

The definition of an acceptable experiment also involved the consideration of the event following a normal breakdown. A multiple low voltage prefire following the initial breakdown excluded that experiment on the basis that the continued energy input during the time of that event significantly influenced the probability of the next event being a failure. An extended breakdown following a normal breakdown, however, added only a very small amount of energy to the flow and therefore did not eliminate that experiment. The breakdown following the extended breakdown was then taken as the second breakdown of the experiment unless it was a multiple low voltage prefire. In general, there were very few multiple low voltage prefires encountered during switch operation over the range of the parameters investigated in this study. There were, however, a significant number of extended breakdowns. Once the two-pulse experiment was defined, all such experiments for each combined data set were identified, and the distribution of the second breakdown voltages in each testing interval became the subject of further analysis.

The quantitative measure of switch performance defined for use in the present investigation was determined from the distribution of the voltages associated with the second breakdown in the two-pulse experiments. This measure of switch performance was cast in terms of two quantities, the cumulative probability, $P_c(V)$, and an associated switch operating voltage, V_{op}. The cumulative probability is the probability, in percent, that the breakdown immediately following a normal breakdown will occur at a voltage lower than the associated operating voltage.

As an illustration, a typical histogram showing the distribution of breakdown voltages of the second breakdown in a set of two-pulse experiments is shown in Figure 2.10. The voltage at which breakdown occurs, grouped in 75-volt intervals, is shown in the first column, and the cumulative probability is shown in the fourth column. For this set of data, the interpolated operating voltage for a one-percent cumulative probability is 8,361 volts, which may be interpreted to mean that for the given set of conditions, there is a one percent chance that a breakdown following a normal breakdown will be below that level.

HOB (VERSION 1.7)
FILENAME : DA169.DAT

ACTUAL FREQUENCY (KHz)	20.144
DIFFERENTIAL PRESSURE (in.H2O)	2.430
UPSTREAM PRESSURE (in.H2O)	2.880
DIVERGENCE ANGLE	3.000
GAP SPACING (in.)	.100
PREVIOUS TOTAL ELAPSED TIME	.000
ELAPSED TIME SINCE RESURFACING	.000
LOW VOLTAGE CUTOFF	2100
INITIAL ARRAY SIZE	2169
NUMBER OF EXPERIMENTS	1557
INITIAL ARRAY MODE	8571
SPREAD ABOUT MODE	200.
VOLTAGE AT .5%	7004.
VOLTAGE AT 1.0%	8141.
VOLTAGE AT 2.0%	8449.
VOLTAGE AT 4.0%	8479.
VOLTAGE AT 5.0%	8488.
VOLTAGE AT 8.0%	8513.
VOLTAGE AT 10.0%	8518.

VOLTS	#	TOTALS	TOTALS %		
4422	1	1	.06	.06	+
4488	0	1	.06	.00	
4554	0	1	.06	.00	
4620	0	1	.06	.00	
4686	1	2	.13	.06	+
4752	0	2	.13	.00	
4818	0	2	.13	.00	
4884	0	2	.13	.00	
4950	0	2	.13	.00	
5016	0	2	.13	.00	
5082	0	2	.13	.00	
5148	0	2	.13	.00	
5214	0	2	.13	.00	
5280	0	2	.13	.00	
5346	0	2	.13	.00	
5412	0	2	.13	.00	
5478	0	2	.13	.00	
5544	0	2	.13	.00	
5610	0	2	.13	.00	
5676	1	3	.19	.06	+
5742	0	3	.19	.00	
5808	0	3	.19	.00	
5874	0	3	.19	.00	
5940	0	3	.19	.00	
6006	0	3	.19	.00	
6072	0	3	.19	.00	
6138	0	3	.19	.00	
6204	1	4	.26	.06	+
6270	0	4	.26	.00	
6336	0	4	.26	.00	
6402	0	4	.26	.00	
6468	0	4	.26	.00	
6534	1	5	.32	.06	+
6600	0	5	.32	.00	
6666	0	5	.32	.00	
6732	2	7	.45	.13	+
6798	1	8	.51	.06	+
6864	1	9	.58	.06	+
6930	0	9	.58	.00	
6996	0	9	.58	.00	
7062	0	9	.58	.00	
7128	0	9	.58	.00	
7194	0	9	.58	.00	
7260	0	9	.58	.00	
7326	1	10	.64	.06	+
7392	1	11	.71	.06	+
7458	0	11	.71	.00	
7524	0	11	.71	.00	
7590	0	11	.71	.00	
7656	0	11	.71	.00	
7722	0	11	.71	.00	
7788	1	12	.77	.06	+
7854	2	14	.90	.13	+
7920	4	18	1.16	.26	+
7986	17	35	2.25	1.09	++
8052	384	419	26.91	23.68	++++++++++++++++++++++
8118	779	1198	89.79	62.88	++
8184	159	1557	100.00	10.21	+++++++++

Figure 2.10 Histogram Showing Breakdown Voltage Distribution of Second Breakdowns in a Set of Two-Pulse Experiments

III. EXPERIMENTAL RESULTS

1. Effect of Accumulated Electrode Operating Time

Figure 3.1 presents an example of the effect of accumulated electrode operating time on switch performance. The frequency distribution curves shown were fit through histograms of normal breakdowns for various sequential test numbers, N. The data were obtained with machined electrodes with electrode divergence angle, θ, of 7.5° and an average gap velocity, $\overline{U}$, of 8.35 m/s.

As seen in the figure, the peak in the frequency distribution curve shifts to lower breakdown voltages and the curve broadens as N increases. This behavior demonstrates that when data for repeat tests on different electrode pairs are combined for analysis, only data for equal N's should be combined as was done in the present study. The reason for the variation with N is apparently the change in electrode surface condition with time, as small pits develop in the vicinity of the minimum gap spacing.

2. Effect of Gas Flow Velocity and Electrode Divergence Angle

Tests were conducted for the various combinations of the average gap velocity ,$\overline{U}$, and electrode divergence angle, θ, shown in Table 3.1. These tests were ducted without a hydrodynamic entry length duct attached to the electrode test section and thus represent the case of minimum hydrodynamic boundary layer development at the point of minimum gap spacing. For each combination of $\overline{U}$ and θ, data sets for N = 1 for various electrode pairs were combined, the two-pulse experiments determined, and histograms were generated to determine the distribution of voltages of the second breakdown for these experiments.

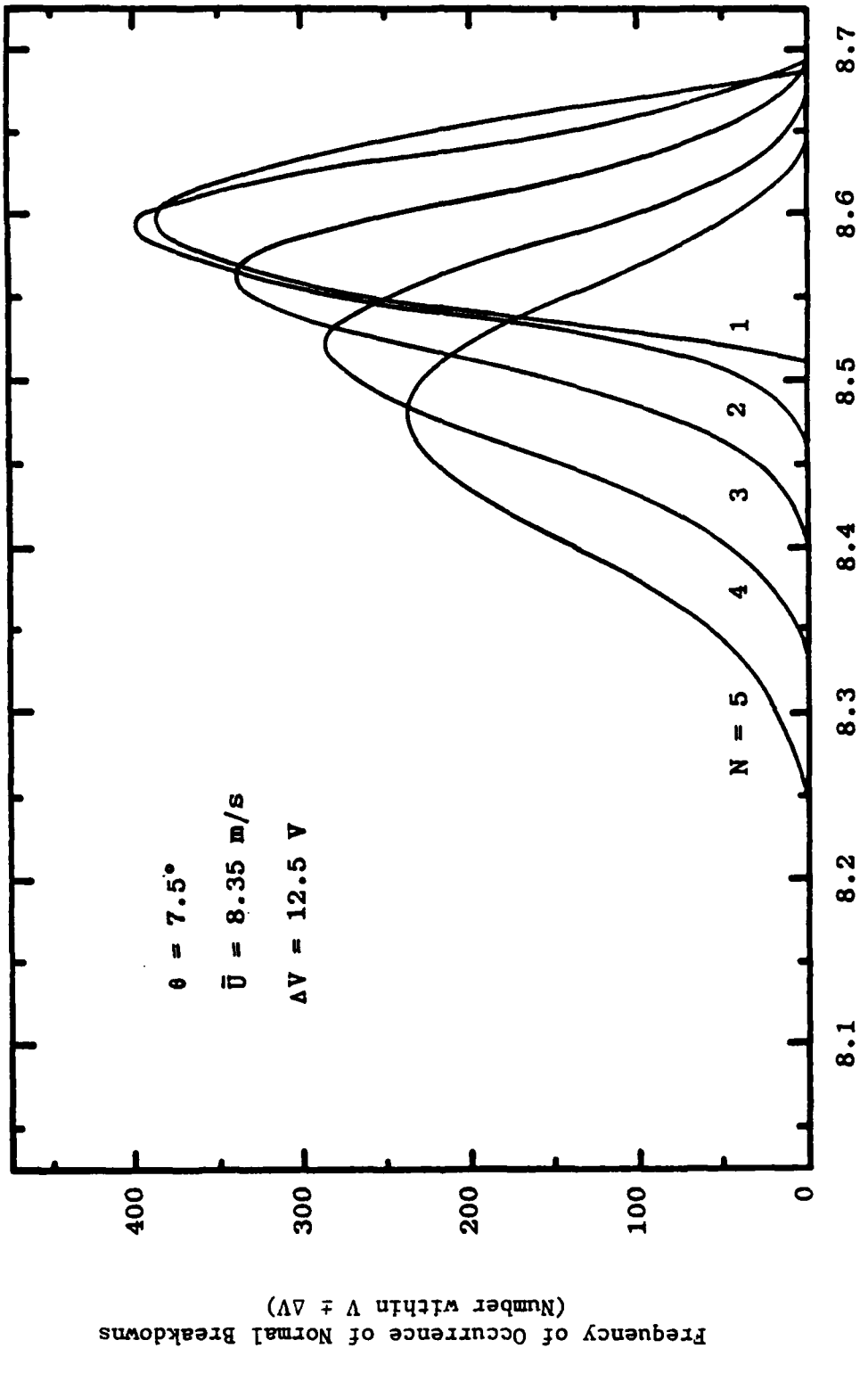

Figure 3.1 Variation of Frequency Distribution with Accumulated Electrode Operating Time

Table 3.1

Data Matrix for Tests with No Entry Length

$\bar{U}$ (m/s) \ θ (°)	5.0	7.5	10.0
4.17	X	X	X
6.24	X	X	X
7.37	X	X	X
8.35	X	X	X
9.74	X	X	
11.10	X		
12.47	X	X	X
13.89	X		
16.53	X		

Figures 3.2, 3.3, and 3.4 present the data for a cumulative probability, $P_c(V)$, of 0.5, 1.0, and 2.0 percent respectively. In each figure the operating voltage, V_{op}, has been plotted versus $\bar{U}$ for the three values of θ. It is seen that, in general, for a given $P_c(V)$ and θ, V_{op} increases rapidly with an increase in $\bar{U}$ until at some value of $\bar{U}$ the operating voltage becomes nearly constant at a value near the mode breakdown voltage. The portion of each curve where V_{op} increases rapidly with an increase in $\bar{U}$ represents primarily prefires, while the flat portion at or near the mode represents primarily normal breakdowns. The velocity at which the rather sharp knee in each curve occurs has been designated as the threshold gap velocity, $\bar{U}_{th}$. Increasing $\bar{U}$ above $\bar{U}_{th}$ essentially results in no improvement in switch performance, thus $\bar{U}_{th}$ is of major interest in conserving purging gas and the power required to pump it through the switch.

Figure 3.5 illustrates the relationship between $\bar{U}_{th}$ and θ for each $P_c(V)$. Each point plotted on the figure was obtained from one of the three preceding figures as the best estimate of $\bar{U}_{th}$ for a given $P_c(V)$ and θ. The curves fit through these points are of the form

$$\bar{U}_{th} = (\bar{U}_{max} - \bar{U}_{min}) \exp(-b\theta) + \bar{U}_{min} \qquad (3.1)$$

This form was selected based on the reasoning that for a given $P_c(V)$, at large θ a minimum threshold velocity, $\bar{U}_{min}$, is required to prevent prefires. Moreover, $\bar{U}_{min}$ is assumed a constant independent of θ since at large θ the electrode geometry becomes two semi-circular cylinders, and the velocity required to prevent prefires becomes a function of electrode radius, not θ. At $\theta = 0°$, $\bar{U}_{th}$ becomes a maximum, $\bar{U}_{max}$, which is a velocity

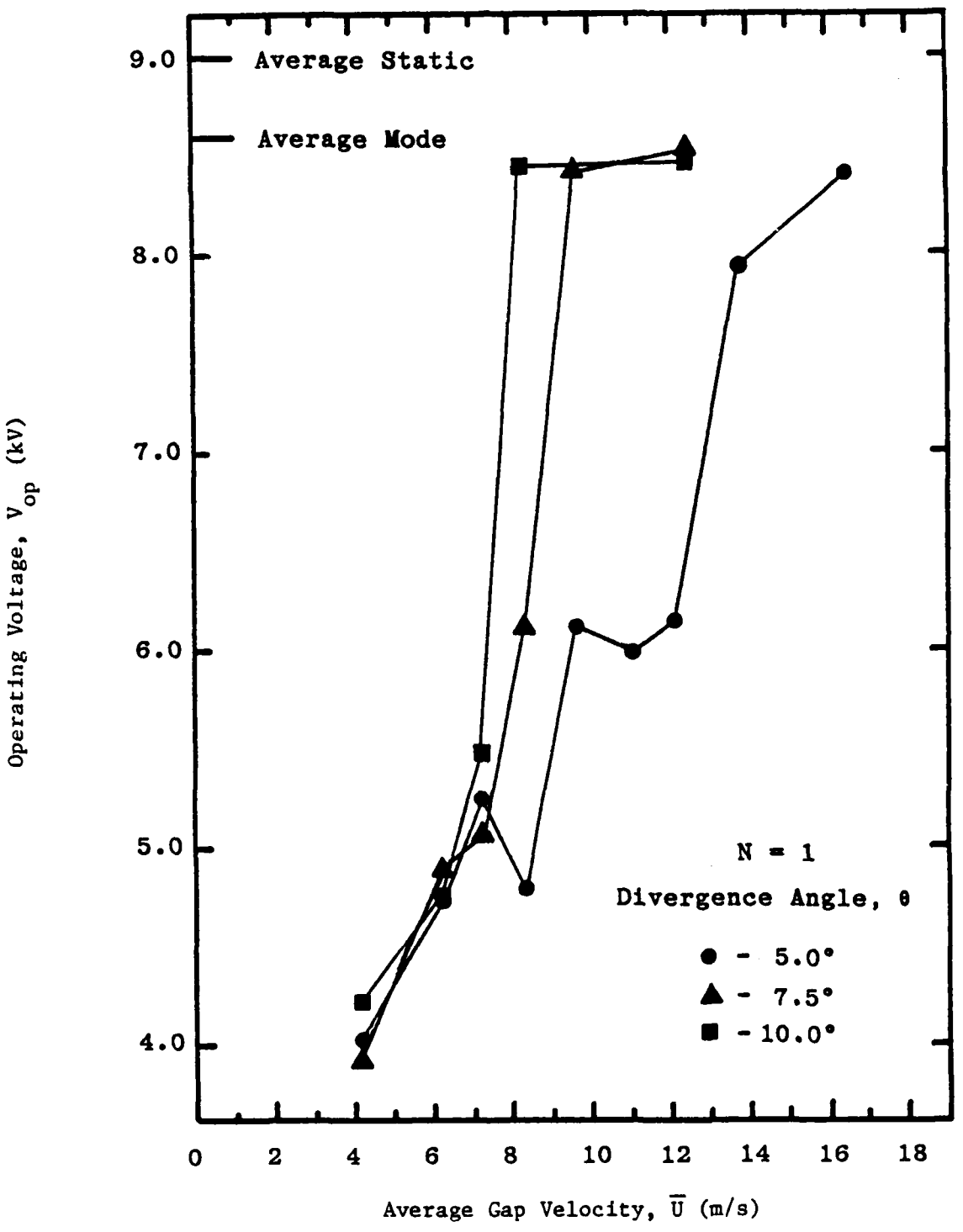

Figure 3.2 Operating Voltage versus Average Gap Velocity for a Cumulative Probability of 0.5 Percent

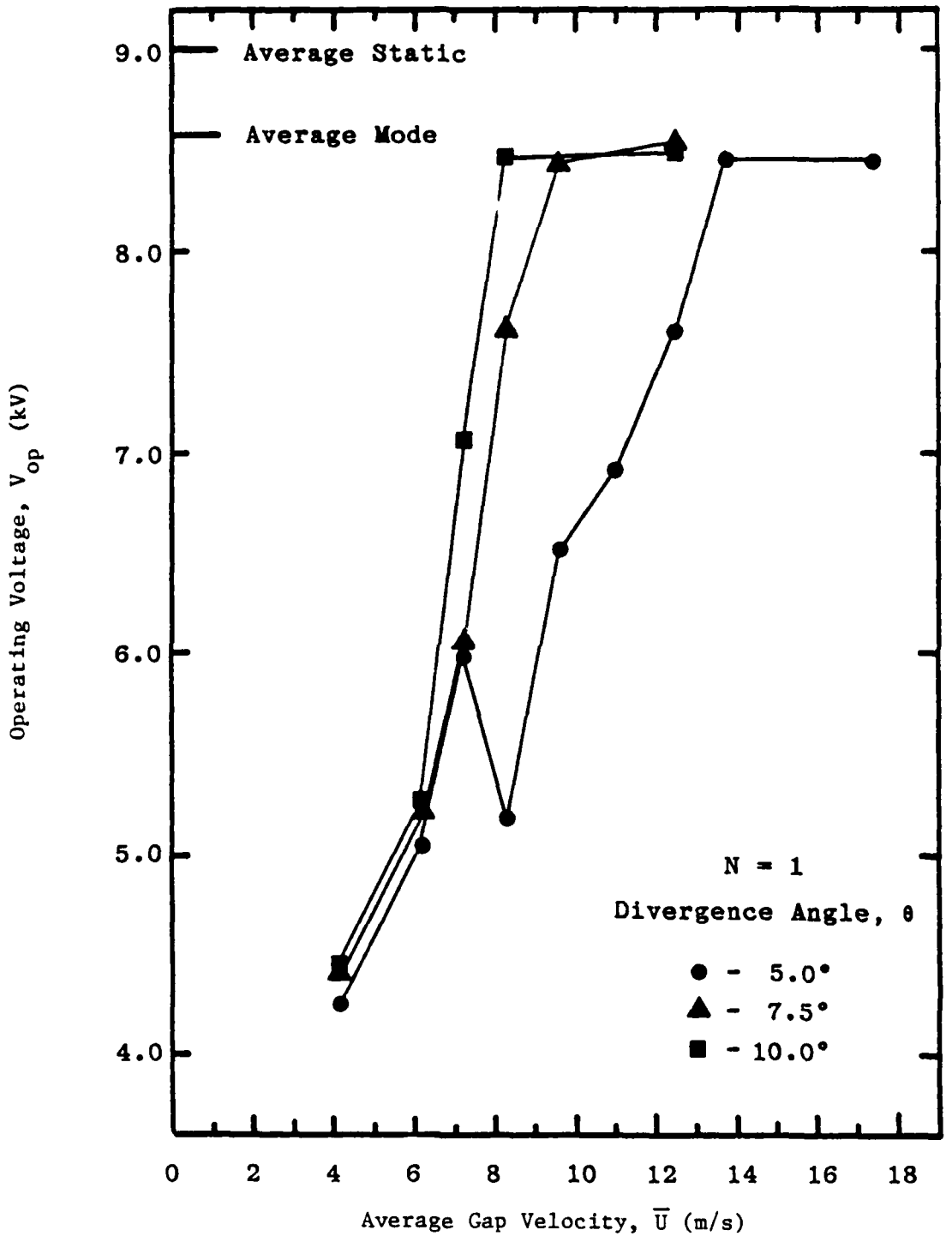

Figure 3.3 Operating Voltage versus Average Gap Velocity for a Cumulative Probability of 1.0 Percent

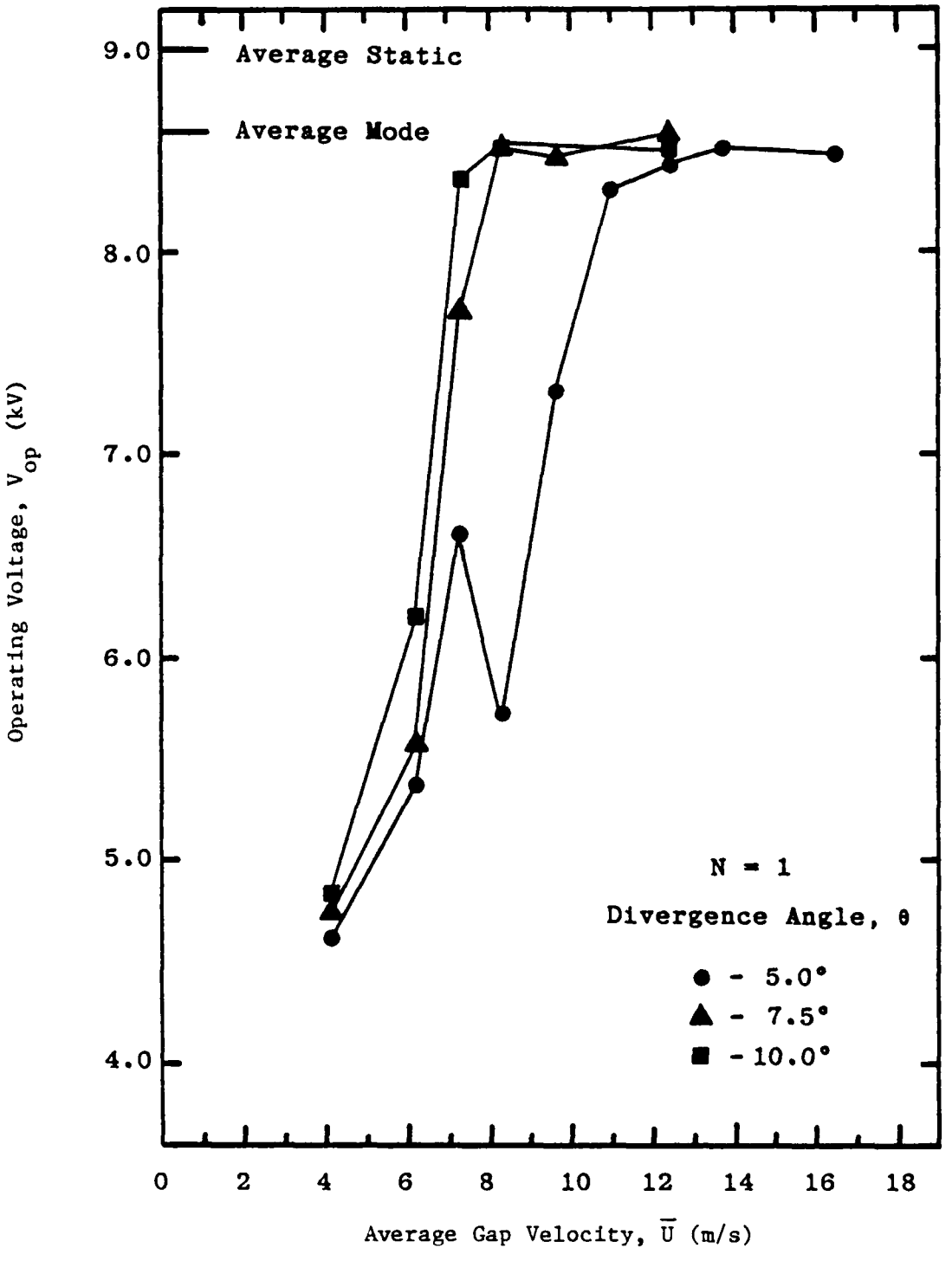

Figure 3.4 Operating Voltage versus Average Gap Velocity for a Cumulative Probability of 2.0 Percent

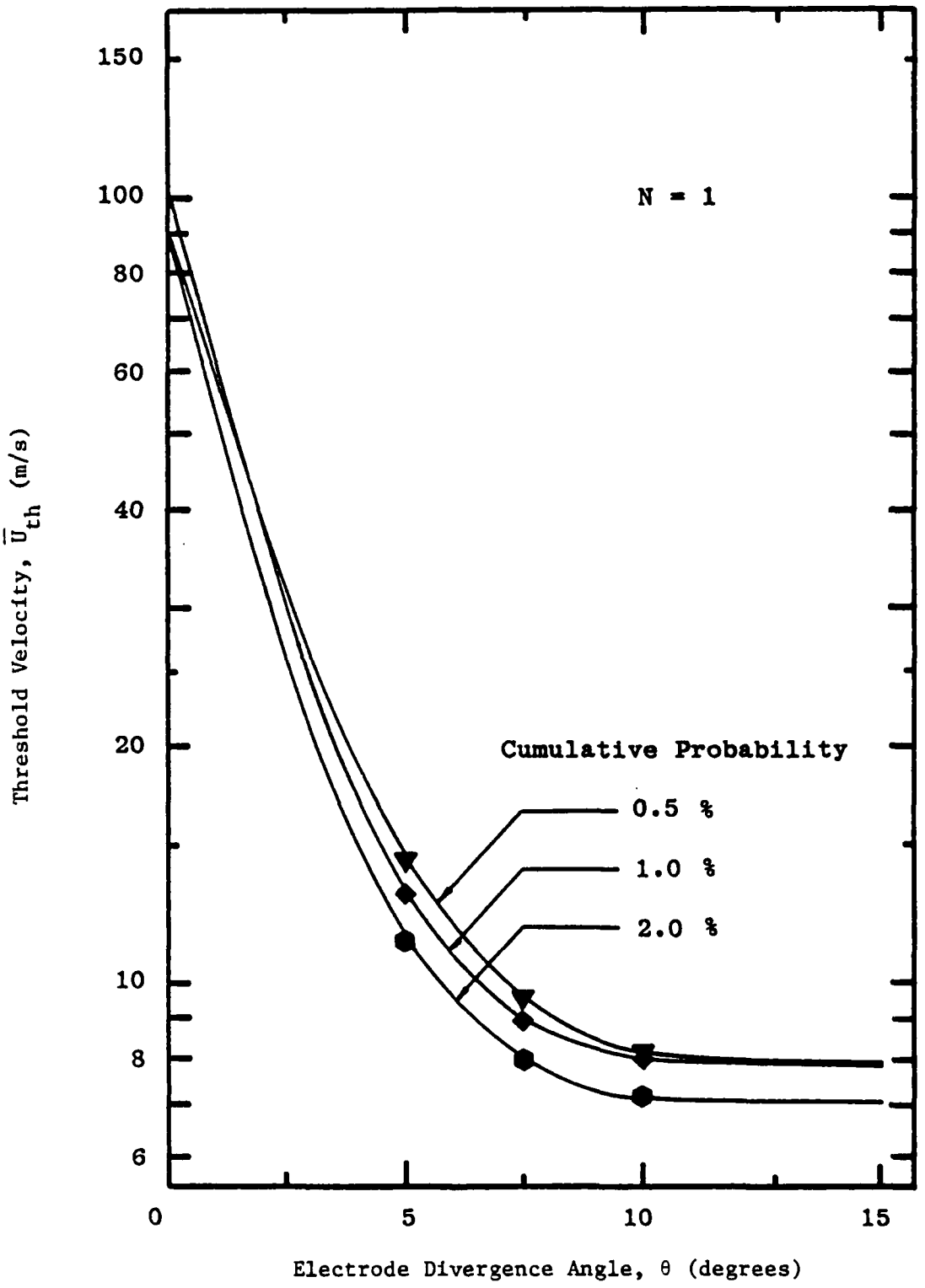

Figure 3.5 Relationship between Threshold Velocity and Electrode Divergence Angle

that essentially must move the hot gas region to a point beyond the downstream end of the electrodes before full voltage is reapplied to the switch. To effect the curve fit for each $P_c(V)$, a value of $\overline{U}_{min}$ was assumed and a least squares analysis was conducted to find $(\overline{U}_{max} - \overline{U}_{min})$ and b. This was repeated for various values of $\overline{U}_{min}$ until the minimum standard error was achieved. The values of the constants are presented in Table 3.2.

Later in the experimental program, the plenum was redesigned to allow investigation of the effects of hydrodynamic boundary layer development on switch performance. In order to determine if the new plenum design would have any effect on the previous results, repeat tests were conducted with the same three values of θ, and with an additional $\theta = 2.5°$ to better define $\overline{U}_{th}$ for smaller angles. Although the qualitative behavior was the same, the data differed quantitatively as shown in Figure 3.6. This figure presents $\overline{U}_{th}$ versus θ for $P_c(V) = 1$ percent, and it can be seen that for $\theta = 5°$, 7.5°, and 10°, $\overline{U}_{th}$ is lower for the second set of tests than it is for the first. The reason for this disagreement is not known. All circuit components, calibrations, and procedures were checked, and no changes had occurred since the first set of tests was conducted. The original plenum was reinstalled, and several tests repeated, and the same lower threshold velocities were obtained. The most plausible explanation for this disagreement is that in the first set of tests there was a leak in the gas supply system, between the laminar flow element and the electrode test section. Such a leak would result in the calculated velocity being higher than the actual through the switch.

Though the data do not agree quantitatively, the results of the second set of tests verify the exponential relationship between $\overline{U}_{th}$ and θ. For

Table 3.2

Constants in Equation (3.1)

P_c(V)	$\bar{U}_{min}$	$\bar{U}_{max}$	b
(%)	(m/s)	(m/s)	(deg^{-1})
0.5	7.8	94.6	0.5160
1.0	7.7	108.9	0.5817
2.0	7.1	94.8	0.6089

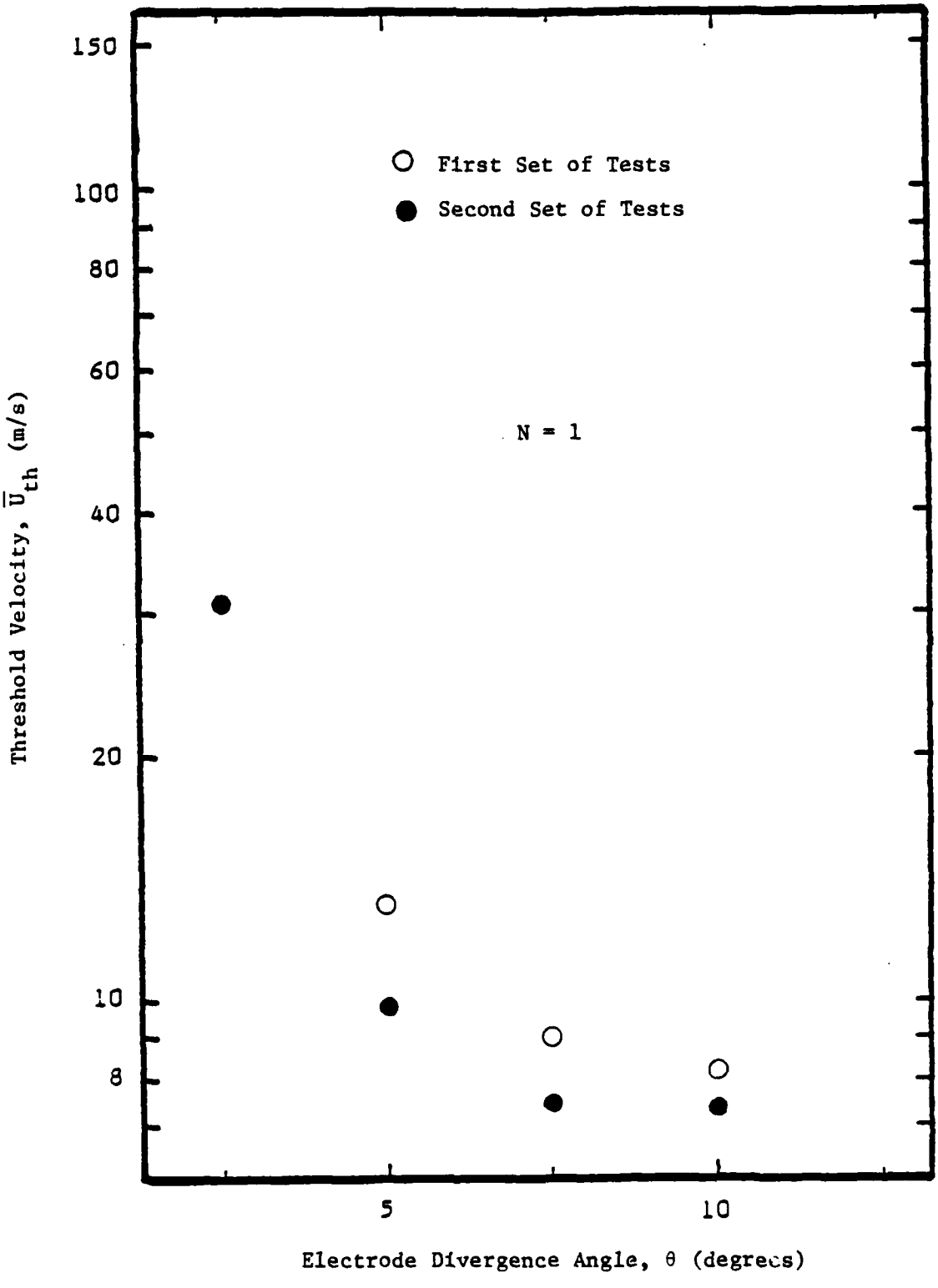

Figure 3.6 Threshold Velocity versus Electrode Divergence Angle for Two Sets of Tests, $P_c(V)$ = 1 Percent

comparison with Table 3.2, the results of the second set of tests give, for $P_c(V)$ = 1 percent, $\bar{U}_{min}$ = 7.3 m/s, $\bar{U}_{max}$ = 202.6 m/s, and b = 0.89 deg^{-1}. Because of the possibility of the leak in the fluid system, these latter values are believed more reliable than those presented in Table 3.2.

The significant finding of the tests conducted to determine the effect of gas flow velocity and electrode divergence angle on switch performance is the exponential relationship between the threshold velocity and the electrode divergence angle. A small amount of divergence in the electrode geometry, as opposed to a uniform gap spacing, can result in a significant reduction in the gas flow rate required to prevent, or minimize, switch prefires.

3. Characterizing Frequency Distribution of Breakdown Voltages

In order to represent quantitatively the distribution of the breakdown voltages of the second breakdown in a combined data set consisting of two-pulse experiments, some effort was spent toward fitting the histograms with frequency distribution curves. It was found that when a combined data set for a given N,θ, and $\bar{U}$ was considered, it was possible to represent accurately the distribution of the breakdown voltages of the second breakdown only for those second breakdowns which were normal breakdowns.

An example, for one of the $\bar{U}$-θ combinations shown in Table 3.1, is presented in Figure 3.7. Here, a Pearson's [2] type I curve was found to represent the histogram of normal breakdown voltages reasonably well. The breakdown voltage distribution of the low voltage breakdowns, most of which represent prefires, is shown in the insert in the lower left-hand portion of the figure.

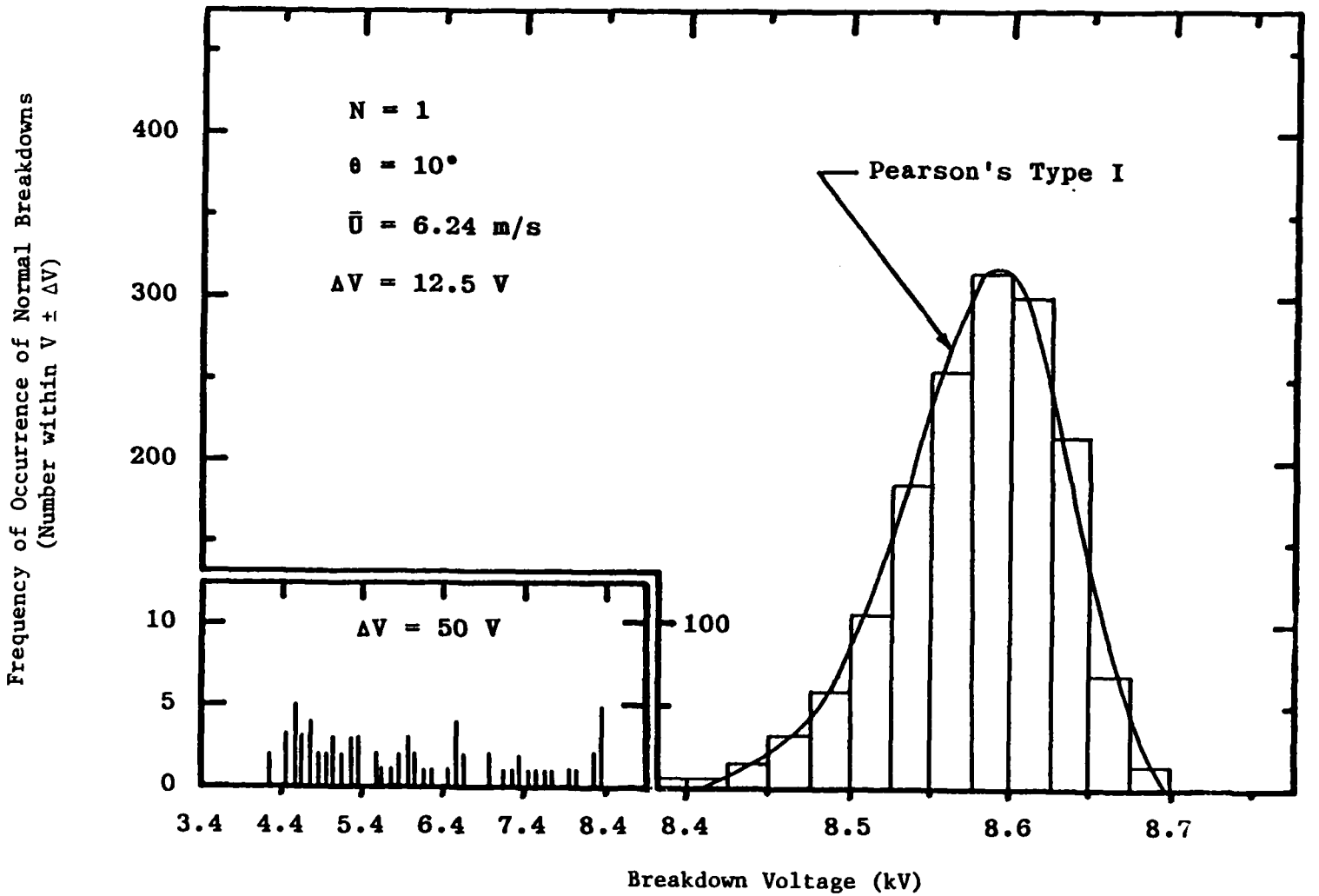

Figure 3.7 Typical Frequency Distribution of Normal Second Breakdowns in a Set of Two-Pulse Experiments with Pearson's Type I Curve Fit

4. Effect of Electrode Design

After the tests to determine the effects of gas flow velocity and electrode divergence angle had been completed, an investigation was conducted to determine if 308 stainless steel rod electrodes would give performance comparable to the 304 stainless steel machined electrodes. Tests were conducted with both electrode types with $\theta = 10°$ and for various $\overline{U}$. Multiple tests were conducted for each $\overline{U}$, each test with a new pair of electrodes, and only one six-second test was conducted on each pair (i.e., N = 1). The two-pulse experiments were determined for each combined data set, and for each electrode type the average and standard deviation in V_{op} for $P_c(V) = 1$ percent were calculated for each $\overline{U}$.

The results are presented in Figure 3.8, where the standard deviation in V_{op} for $P_c(V) = 1$ percent is plotted versus $\overline{U}$ for both electrode types. It can be seen in the figure that the standard deviation in operating voltage is greater for the rods than it is for the machined electrodes at the various flow velocities, especially near the threshold velocity. For this reason the testing program was continued with the machined electrodes.

One possible explanation for the different behavior may be the difference in material composition. However, there is only a minor difference in the AISI specification [3] for 304 and 308 stainless. The allowable range for chromium is 18-20 percent for 304 and 19-21 percent for 308, while the allowable range for nickel is 8-12 percent for 304 and 10-12 percent for 308. These are the only composition differences and are probably insignificant in determining switch behavior. Another possible

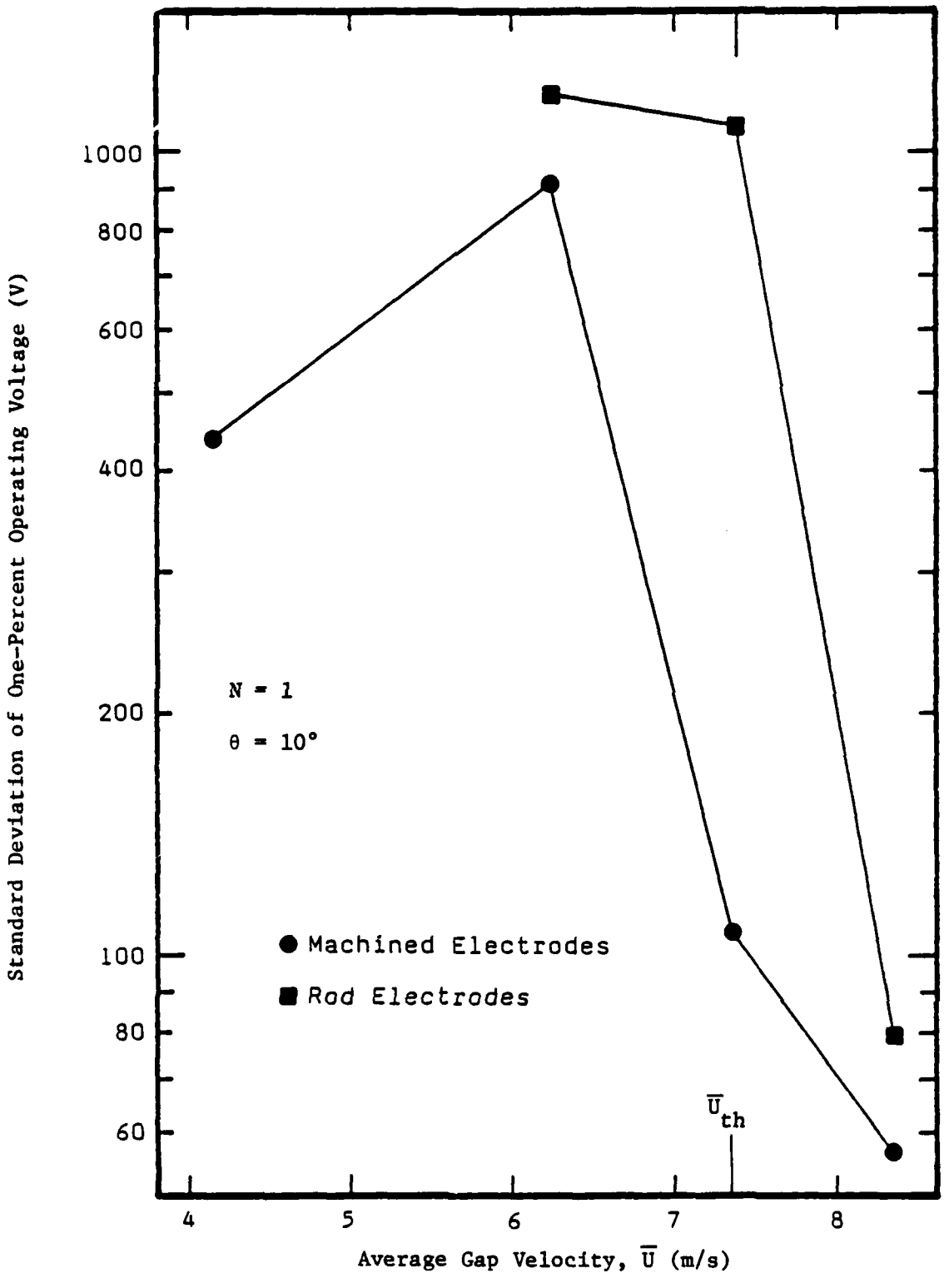

Figure 3.8 Standard Deviation of One-Percent Operating Voltage versus Average Gap Velocity for Rod and Machined Electrodes

explanation is that structural changes, resulting from small cracks or residual stresses introduced by the bending process, caused the difference in behavior.

5. Effect of Hydrodynamic Boundary Layer Development

Figure 3.9 presents V_{op} for $P_c(V) = 1$ percent plotted versus $\overline{U}$ for $\theta = 5°$ for entry lengths of 0, 6.19, 17.46, and 27.78 cm. Figure 3.10 presents the results for $\theta = 10°$, with the same entry lengths plus an additional entry length of 57.3 cm. Both figures show that the curves of V_{op} versus $\overline{U}$ with an entry length have the same general characteristics as those for no entry length, in that they still exhibit a sharp rise until a threshold velocity, $\overline{U}_{th}$, has been reached and at higher velocities the voltage is nominally constant.

From Figures 3.9 and 3.10, $\overline{U}_{th}$ for each θ was determined and plotted versus entry length as shown in Figure 3.11. The smooth curves were drawn through the data by eye. Data were not obtained for $\theta = 5°$ with an entry length of 57.3 cm because had a test for $\overline{U}$ substantially below $\overline{U}_{th}$ been conducted in order to determine $\overline{U}_{th}$, the electrode holders and entry length could have been damaged as a result of severe switch failure. From Figure 3.11 it is seen that for either θ there is an optimum entry length, which requires a minimum $\overline{U}_{th}$ to achieve the optimum performance. This optimum entry length is seen to be between 10 and 20 cm.

This result is surprising because initially it was anticipated that the added entry lengths would progressively deteriorate the performance of the switch. This was thought because the increasing development of the laminar hydrodynamic boundary layer would slow the purging of the low density, hot

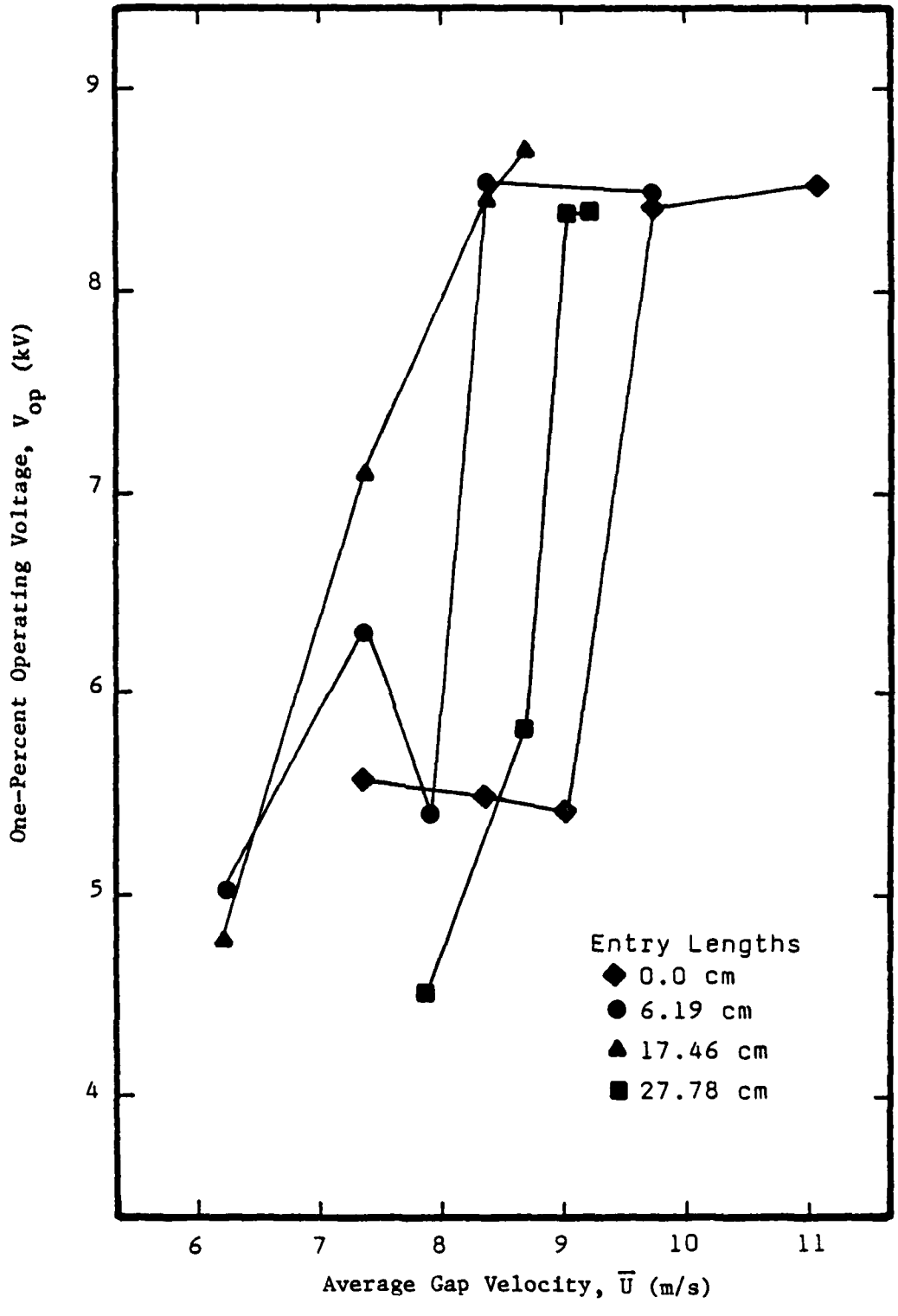

Figure 3.9 Effect of Average Gap Velocity on One-Percent Operating Voltage for Various Entry Lengths for $\theta = 5°$

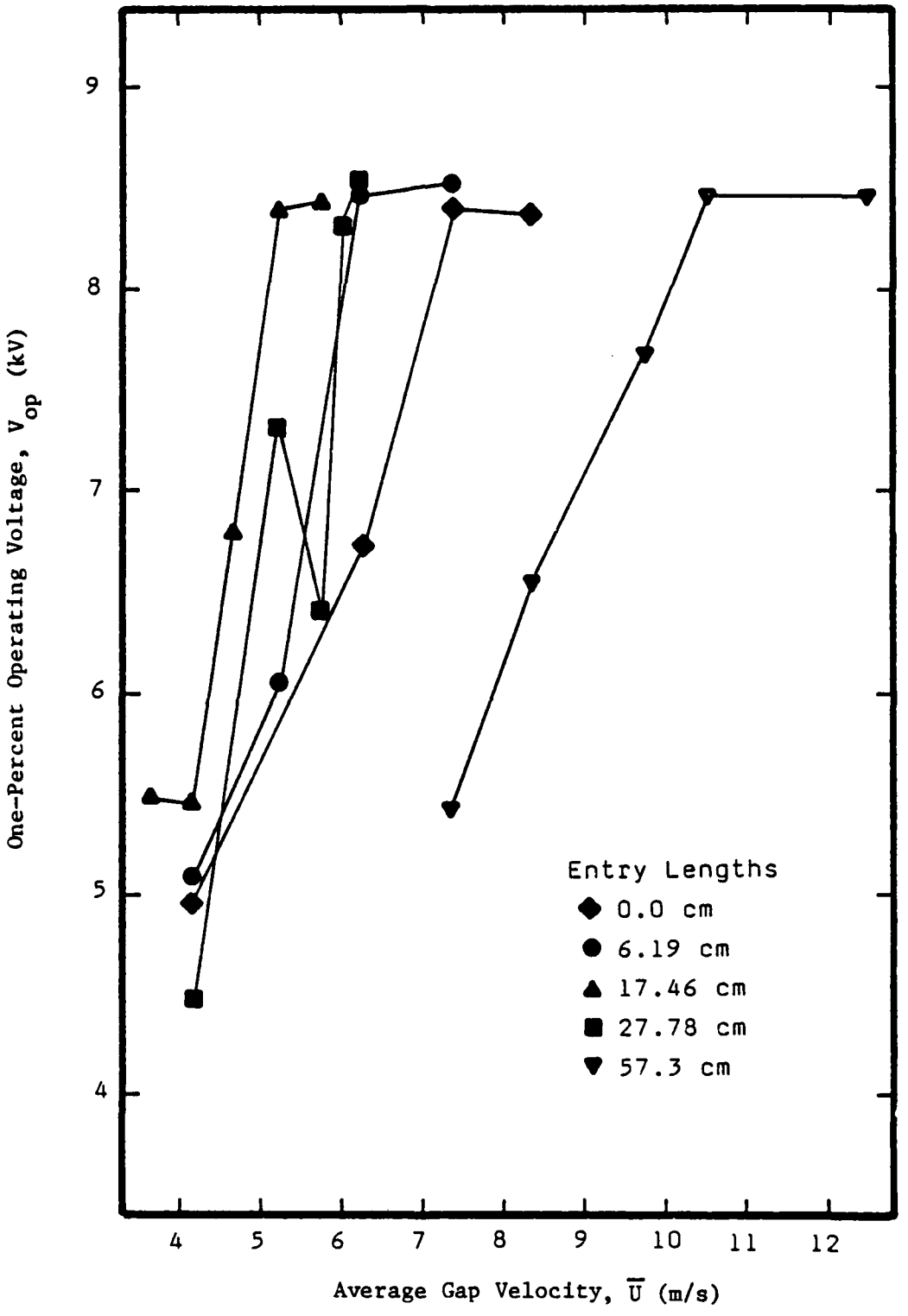

Figure 3.10 Effect of Average Gap Velocity on One-Percent Operating Voltage for Various Entry Lengths for $\theta = 10°$

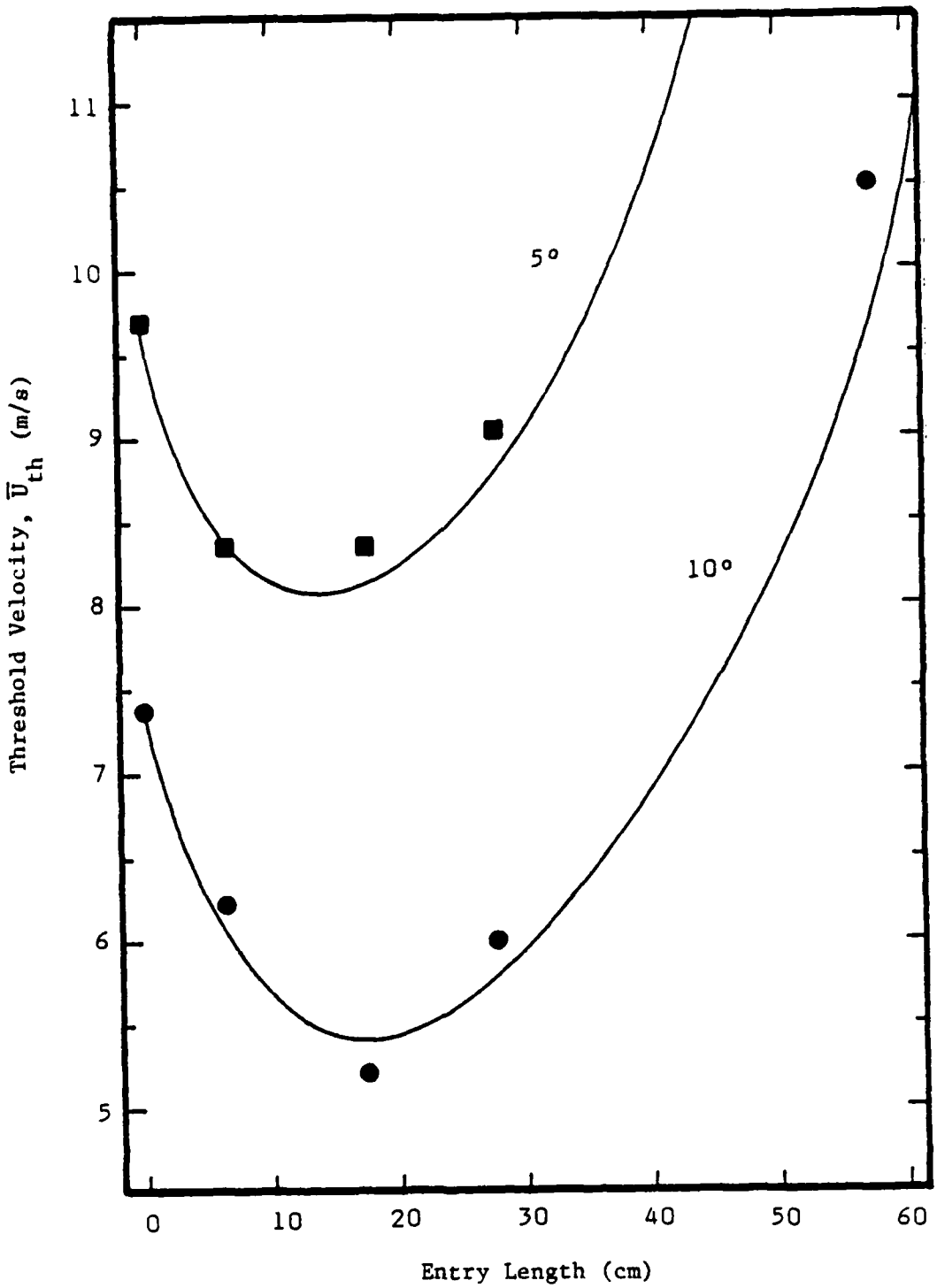

Figure 3.11 Effect of Entry Length on Threshold Velocity

gas at an increasingly greater distance from the surface of the electrodes. From the above results it is obvious that this is not the case.

Apparently there is some optimum laminar boundary layer development responsible for these results. To document the boundary layer development, a hot-wire anemometer traverse at the minimum gap spacing was conducted for all entry lengths to obtain the velocity profiles. The results of the traverse are shown in Figure 3.12. Each individual profile was plotted with the vertical axis being the distance across the gap at the minimum separation point, and the horizontal axis being the local flow velocity normalized with the centerline velocity. The profiles in the left column are for an average velocity below $\overline{U}_{th}$ causing nearly hydrodynamically fully-developed flow, the profiles in the center column are for $\overline{U}_{th}$, and the profiles in the right column are for some average velocity greater than $\overline{U}_{th}$. The rows represent the entry lengths used to generate the profiles. Figure 3.12 shows that at $\overline{U}_{th}$, the profiles are very nearly the same shape except for the profile with the entry length of 17.46 cm, which is approximately the optimum entry length seen in Figure 3.12. This suggests that a certain density distribution must be attained across the gap before the maximum voltage can be applied and that the velocity profile for the optimum entry length gives this density distribution.

6. Effect of Turbulence

The case selected for the investigation of the effect of turbulence was for $\theta = 10.0°$ with the 27.78-cm entry length. At the flow velocities tested the flow was laminar, therefore, turbulence was artificially generated with a screen (1.0 mm square openings separated by 1.0 mm) located 7.62 mm upstream of the minimum gap spacing.

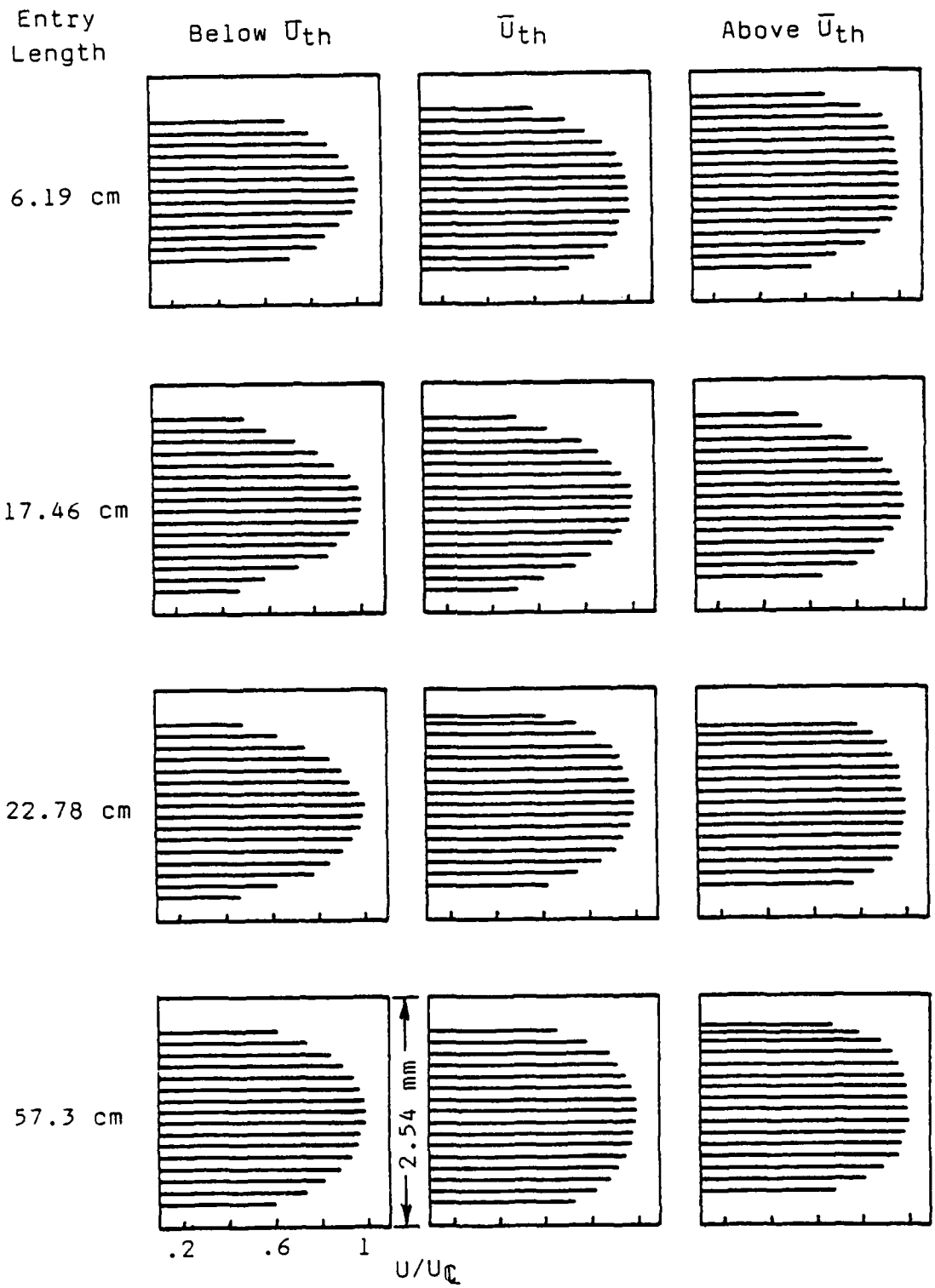

Figure 3.12 Velocity Profiles in the Plane of Minimum Gap Spacing

The turbulence intensity was measured with the hot-wire anemometer both with and without the screen over the range of velocities tested. The hot-wire probe was located at the flow centerline at the minimum gap spacing. The results of this test are shown in Figure 3.13. From this figure it is seen that at $\overline{U}$ = 3.25 m/s, the turbulence intensity is almost the same for both the laminar and the turbulent cases. Above 3.25 m/s the difference increases significantly.

The resulting V_{op} for $P_c(V)$ = 1 percent versus $\overline{U}$ curves are compared in Figure 3.14. From this graph it is seen that the curve for the turbulent case is considerably different from that for the laminar case. The normally well-defined knee of the curve for the laminar case is replaced by a more gently increasing curve suggesting that the increase in turbulence intensity has less effect after the steep initial rise. After $\overline{U}_{th}$ has been attained, the nominally constant voltage is basically the same for both the turbulent and laminar cases. The most apparent reason for the improvement is that turbulence mixes the flow and therefore disperses the hot gas more efficiently. A comparison between laminar and turbulent flow can be seen from the series of example interferograms presented in Figure 3.15. The camera speed for both cases was approximately 4,000 pictures per second with every other picture being shown in the figure. The flow velocity was 4.17 m/s for both cases. The shape and character of the hot gas region for the laminar case can be seen to remain about constant through the sequence, while the shape of the hot gas region for the turbulent case is more irregular and can be seen to change more dramatically through the sequence. Referring to Figure 3.14, a large difference in operating voltage, V_{op}, can be seen for a flow velocity of 4.17 m/s. This agrees with what can be seen

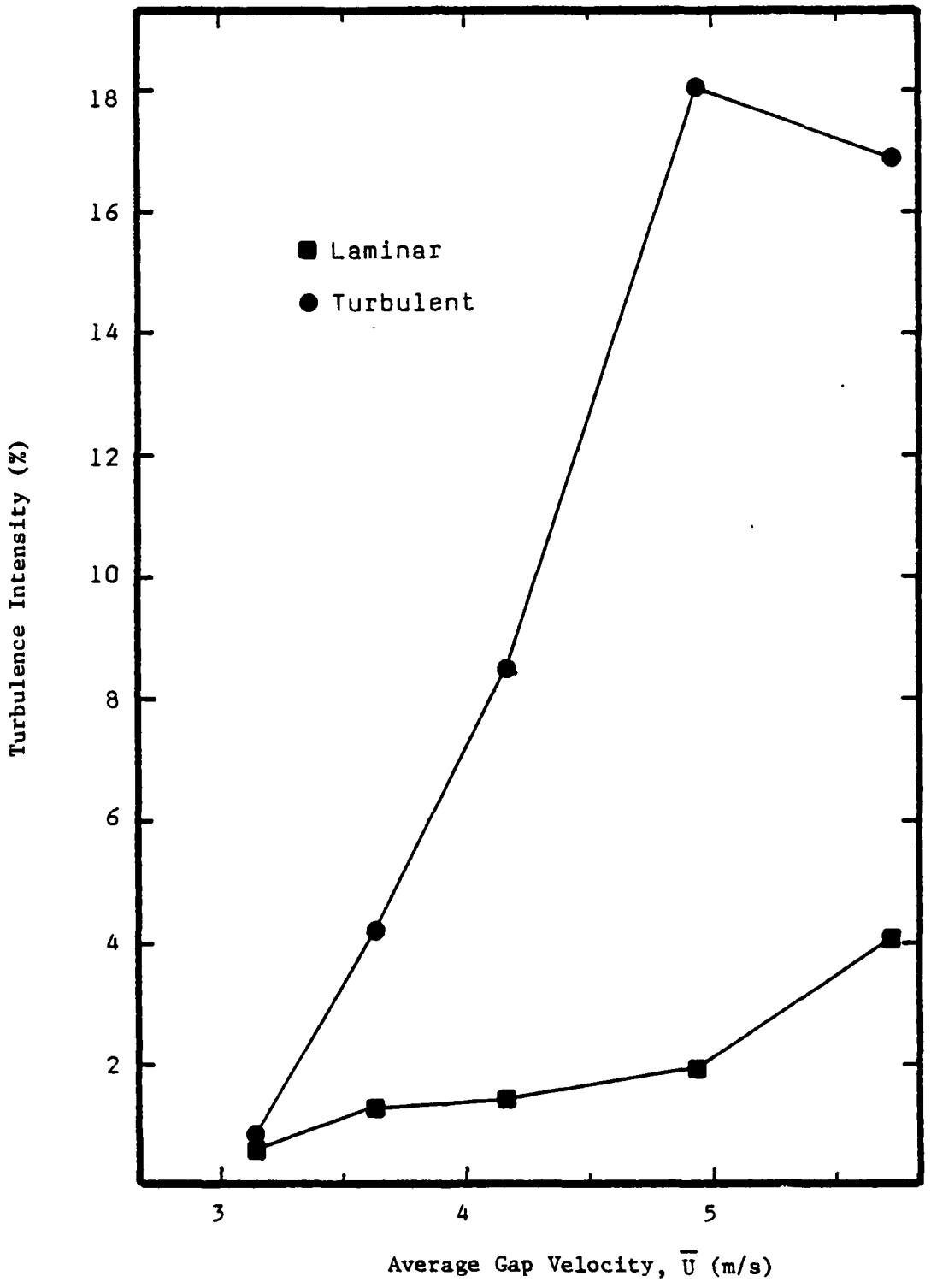

Figure 3.13 Turbulence Intensity versus Average Gap Velocity for Laminar and Turbulent Flow, Entry Length = 27.78 cm, $\theta = 10°$

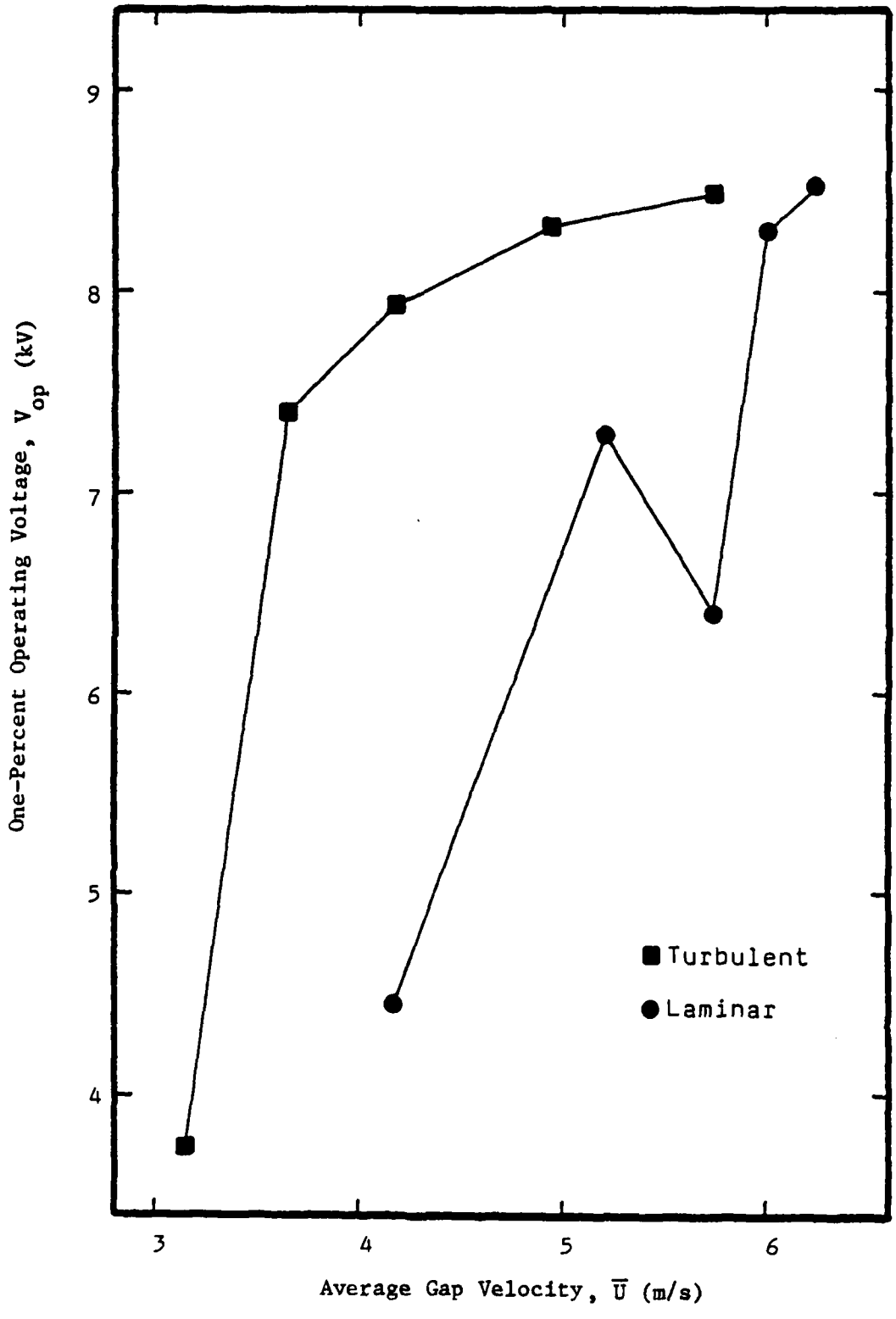

Figure 3.14 Effect of Average Gap Velocity on One-Percent Operating Voltage for Laminar and Turbulent Flow, Entry Length = 27.78 cm, $\theta = 10°$

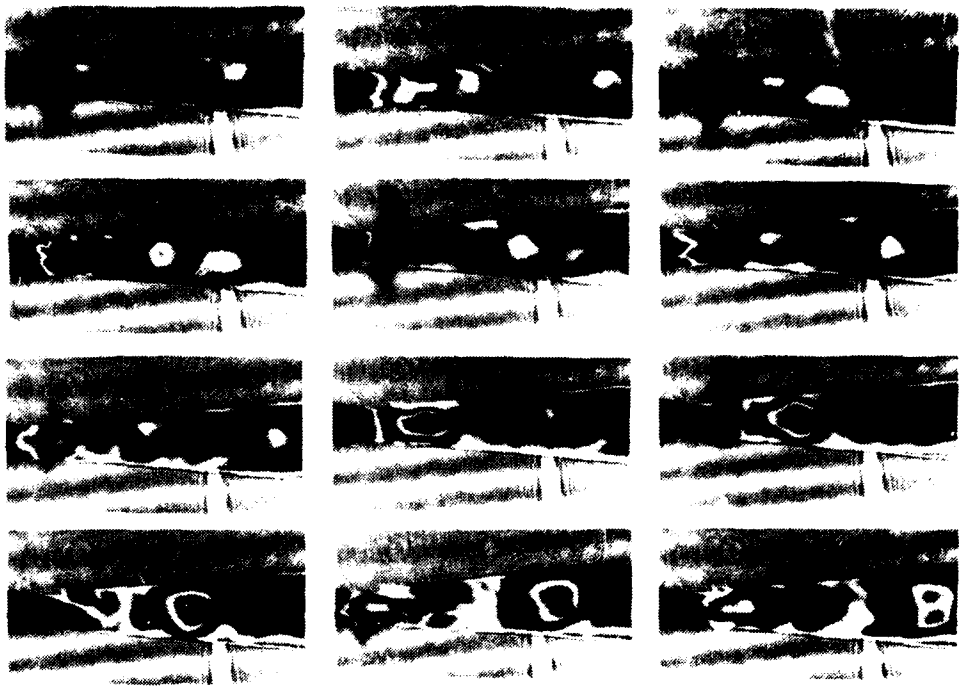

(a) Laminar Flow

(b) Turbulent Flow

Figure 3.15 Interferograms for Laminar and Turbulent Flow, Entry Length = 27.78 cm, $\bar{U}$ = 4.17 m/s, θ = 10°

in Figure 3.15, that is, there is a larger number of prefires (vertical dark spots) in the laminar case as compared with the turbulent case.

7. Multidimensional Flow Visualization

Most of the interferograms obtained in the present study, examples of which were presented previously, were obtained in the usual manner of passing a single light beam, oriented normal to the plane of the electrodes, through the electrode test section. For two-dimensional density fields, such interferograms can be used to provide quantitative data on density distribution. However, the hot gas region produced by a circular arc is three-dimensional, and a single-beam interferogram provides information only on the integrals of unknown density variations over unknown optical path lengths. No information is provided on the extent of the heated region normal to the flow or on whether or not the heated region is symmetrical or asymmetrical, and such information would be of interest in model studies.

To provide additional insight into the three-dimensional nature of the hot gas region produced by an arc, an exploratory investigation was conducted to conceive, design, and construct a device that would provide multiple, simultaneous interferograms of the interelectrode region as viewed from different angles. The resulting device permitted two beams to be sent through the electrode test section. Each beam could be directed at an angle of 45° to the plane of the electrodes, or one beam could be normal to the plane of the electrodes and one at 45°. The beams emerged from the device parallel, but displaced transversely, so that the two interferograms could be recorded side-by-side in a single frame with a high-speed camera.

A beam crossing the plane of the electrodes at 45° was produced by a system of four, 1/20-wave flat mirrors. The resulting multiple reflections lengthened the beam path, and one design requirement that had to be met was that the additional path length had to be less than the coherence length of the laser in order that fringes be produced upon recombination of the multiply-reflected beam with the reference beam of the interferometer. The mirrors were cemented to L-shaped mounts that were clamped to a vertical aluminum plate. This plate was attached to a horizontal plate which rested on a padded track allowing the assembly to be easily displaced for access to the electrode test section.

In positioning the eight mirrors when two beams were used, each at 45° to the plane of the electrodes, the number of variables which had to be dealt with was 32 (4 mirrors × 2 dimensions of translation of the base plate × 2 dimensions of rotation × 2 beams). One mirror in each beam had the capability of adjustment by three micrometers to give fine adjustment.

To check for parallelism of the two beams entering the high-speed camera, a card was placed in the interferometer to partially block the reference beam. The camera was removed from the optical rail, and a 480-mm focal length lens was used to bring the light to a focus. When the images for all three beams formed at the focal point of the lens, they were parallel and would produce fringes. The reference beam covered so much larger a cross section than the two other beams that it had to be attenuated when checking for parallelism so the light through the test section could be seen. When the beams emerging from the test section had been set parallel, fringes could be seen on a card placed in front of the lens.

Adjustment of the micrometers of the adjustable mirror in each beam moved the fringes to bring a single bright fringe to cover the entire image of the test section. The adjustment of micrometers was done for each beam passing through the test section. The camera was then placed in the beam emerging from the interferometer, and the photographic exposure of the flow was made in the usual way as for single beam interferograms.

Figure 3.16 presents an example sequence of interferogram pairs, each pair showing the interelectrode region as viewed from two different angles simultaneously. The interferograms in the left column were produced by a beam oriented 45° to the plane of the electrodes, and those in the right column were produced by a beam oriented perpendicular to the plane of the electrodes. The time sequence is from top to bottom, and the flow direction is from left to right. The average gap velocity, $\overline{U}$, is 6.24 m/s and the electrode divergence angle, θ, is 5°. A Fastax, 16 mm camera was used to obtain the interferograms.

The dark spot in the first pair of interferograms at the top of the figure is the arc discharge. The interferogram on the left shows the hot gas from the previous discharge which is not visible in the interferogram on the right due to the different viewing angle. It will be noted that the interferograms for the 45° view are about one-half wave out of phase with the interferograms for the normal view, in that the background illumination is light for the former and dark for the latter. This also causes corresponding fringes for the two cases to be out of phase by the same amount. It is seen that for any pair of interferograms, the overall size of the hot gas region is about the same whether viewed normally or at 45° to the plane of the electrodes. However, there are differences in the

Figure 3.16 Sequence of Interferograms Obtained with Two Different Viewing Angles, $\bar{U}$ = 6.24 m/s, θ = 5°

fringe patterns which indicate that the integral of the density over the optical path length is different for the two views, and therefore the density distribution and/or shape of the hot gas region is not symmetrical. It would be expected, of course, that as the hot gas region is displaced downstream, the region would be distorted in the flow direction due to the effects of the boundary layers. However, even the pair of interferograms immediately following the arc, obtained at a time of the order of 250 μs following the arc discharge, already show an asymmetric character.

IV. RESULTS OF NUMERICAL MODEL

1. Background

As has been seen in the experimentally obtained interferograms presented previously, the thermal energy released into the flow stream by the arc produces a high temperature, low density region which is eventually flushed from the gap. Immediately after the discharge, the hot gas region is essentially symmetrical about the axis of the arc, but as it is carried downstream the hot gas mixes with the cooler incoming gas stream, spreads out and decreases in temperature. The objective of the numerical modeling portion of this project was to develop a computer algorithm capable of predicting the post-arc density field for laminar flow in the gap of a gas-blown switch as a function of time. The algorithm was to include the effects of switch geometry, heat transfer and compressibility. In general, a three-dimensional, transient, elliptic solution to the Navier-Stokes equations and the energy equation was proposed. It was further envisioned that a finite-difference method incorporating a body-fitted coordinate scheme and a moving grid technique would form the basis of the solution algorithm.

The use of a body-fitted coordinate system was intended to facilitate the matching of the finite-difference grid to arbitrary three-dimensional switch geometries. In general, a body-fitted coordinate scheme capable of generating grids for arbitrary three-dimensional geometries produces non-orthogonal grids, and thus requires that the finite-difference equations be developed for a non-orthogonal coordinate system. The advantage of a non-orthogonal, or body-fitted, coordinate system is that fluid-

surface interactions are generally predicted more accurately if the grid "fits" the geometry of the calculation domain than if a "blocked out" fixed grid is utilized to simulate the flow geometry.

The high temperature region produced by the arc moves with the gas flow through the switch. Thus, the moving grid concept was to be introduced to allow a region of fine grid mesh that could move along with the hot gas. Such an arrangement would allow the total number of grid points or computational control volumes to be minimized while retaining an adequately fine grid near the hot region where large gradients of density and temperature are anticipated. The alternative is to make the grid fine in the entire region where the hot region is expected to pass.

2. Computational Algorithm

Much time was spent on the development of an algorithm incorporating body-fitted coordinates and a moving grid scheme. However, the transformed equation set necessary for the body-fitted coordinates proved difficult to solve, and the algorithm exhibited convergence problems. Therefore, it was decided to use a more typical finite-difference scheme based on a rectangular Eulerian coordinate system. The finite-difference algorithm used to make the predictions shown in this report is a modified version of the Patankar-Spalding Simple Method for Pressure Linked Equations (SIMPLE). This method has been used for several years and is well documented [4,5,6].

To date, only two-dimensional computations have been carried out for the spark gap switch. This does not represent a limitation of the algorithm, but rather, a limitation in the period of performance of the present research project. The algorithm embodies an elliptic, finite-

difference solution of the two-dimensional, transient conservation equations for mass, momentum, and energy. These equations are shown below.

Conservation of Mass

$$\frac{\partial \rho}{\partial t} + \nabla \cdot (\rho \bar{V}) = 0 \tag{4.1}$$

Conservation of Momentum

$$\rho \frac{\partial \bar{V}}{\partial t} + \rho(\bar{V} \cdot \nabla)\, \bar{V} = -\nabla p + \rho \bar{B} - \nabla \times [\mu(\nabla \times \bar{V})] + \nabla[(\lambda + 2\mu)\, \nabla \cdot \bar{V}] + S_{\bar{V}} \tag{4.2}$$

Conservation of Energy

$$\rho \frac{\partial T}{\partial t} + \rho(\bar{V} \cdot \nabla)\, T = \nabla \cdot (\Gamma_T \nabla T) + S_T \tag{4.3}$$

The symbols in the above equations are defined as follows:

$\bar{V}$	the velocity vector
p	the static pressure
$\bar{B}$	the body-force vector
T	temperature
ρ	the fluid density
μ	the dynamic viscosity
λ	the second coefficient of viscosity
Γ_T	the transport coefficient for energy
t	time
$S_{\bar{V}}, S_T$	any additional sources (or sinks) of the respective quantity
∇	the vector differential operator

3. Computational Results

The computational results presented here were carried out for transient, two-dimensional, laminar flow through a switch gap with an included angle of 5°. The flow was assumed to be symmetrical about the centerline of the flow channel. This assumption made possible the use of a grid that covers only one-half of the flow channel. The grid used for the computations, shown in Figure 4.1, consisted of 78 control volumes in the flow direction and 23 control volumes in the cross stream direction. The channel geometry was simulated by blocking out computational cells as needed. The darkened areas in Figure 4.1 represent the channel walls or electrodes. Both sides of the flow channel are shown in Figure 4.1 for clarity even though the grid extends only half way across the channel.

Figure 4.2 presents a sequence of interferograms obtained during the experiments. The switch was operating at a low repetition rate of about one pulse per second so that the electrodes were at a temperature near ambient. The average gap velocity, $\overline{U}$, is 5.5 m/s and the electrode divergence angle, θ, is 5°. The interferograms were obtained with a Dynafax drum camera, which uses 35 mm film strips, 0.76 m long, and has a maximum speed capability of about 20,000 pictures per second. The interferograms shown in Figure 4.2 were obtained at a camera speed of 8,240 pictures per second. The time elapsed from the beginning of one interferogram to the next is approximately 122 μs, and the exposure time for each interferogram is approximately 6.5 μs. The prediction of the model will be compared with this sequence of interferograms.

The initial condition for the computer solution was provided by superimposing a region of high temperature gas on the steady-state solution

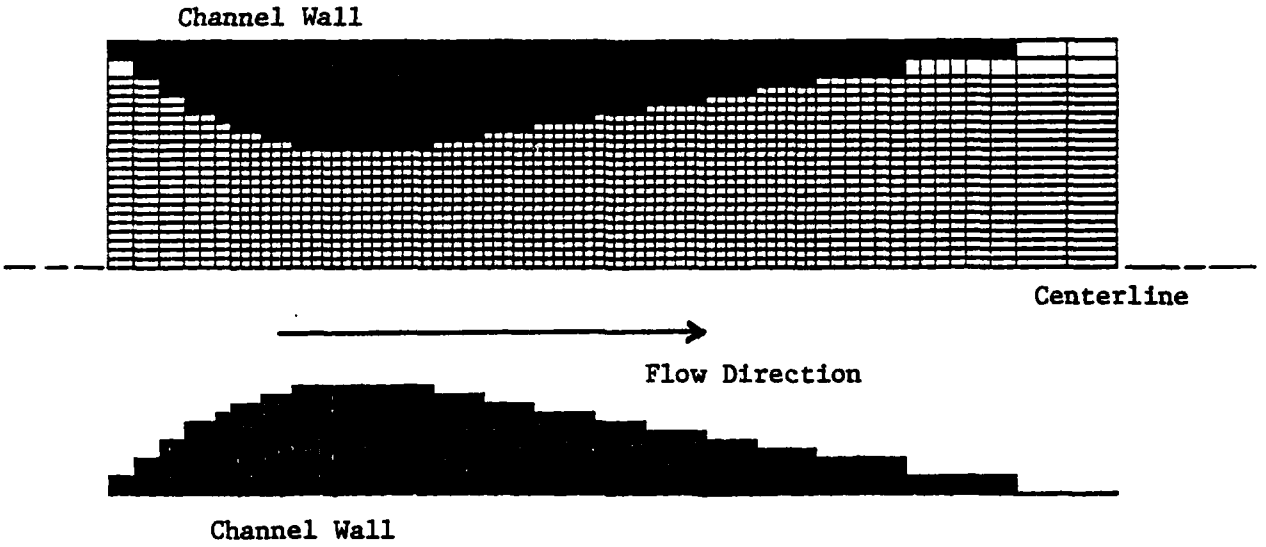

Figure 4.1 Finite-Difference Grid Used in Computations of Flow in Channel with $\theta = 5°$

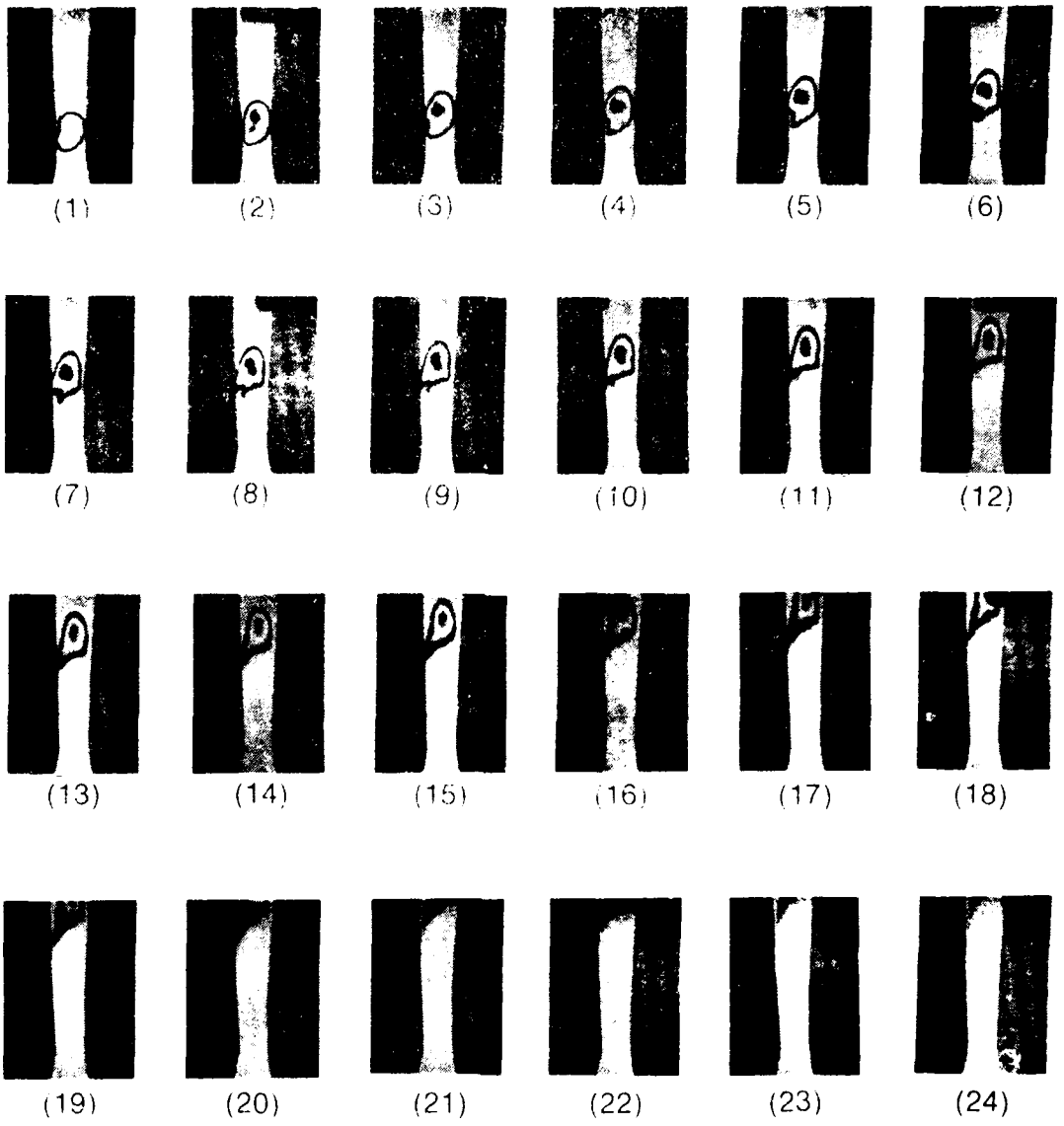

Figure 4.2 Interferograms for $\bar{U}$ = 5.5 m/s, θ = 5°

for isothermal flow through the channel. The cross-section of the initial region was assumed to be the same as that shown in the first interferogram of Figure 4.2. However, since the simulation is two-dimensional, the hot gas region is infinitely long perpendicular to the flow direction, and the volume of the region is larger, with respect to the mass flow rate through the channel, than it is for the actual flow. For the initial hot gas region, it was assumed that recombination of the ionized gas had been completed, and that the temperature over the region was uniform. The electrode temperature was constant at the ambient temperature to correspond with the experimental conditions employed when the interferograms of Figure 4.2 were obtained. For the first interferogram shown in Figure 4.2, the average temperature of the hot gas region was estimated to be about 200 K above ambient. Thus, in the initial computer run a value of 500 K was used for the starting temperature.

The computations were performed for 100 time steps of 12.2 μs each. The results were stored for every tenth time step, or for every 122 μs, approximately the time lapse between the interferograms shown in Figure 4.2. The computations required 512 K of memory and approximately 12 minutes of processor time on an IBM 3033 computer.

Figure 4.3 presents the computed interferograms for an average gap velocity, $\overline{U}$, of 5.5 m/s. These simulated interferograms were obtained by dividing the predicted density range into nine equal increments of density. The lowest density range is shaded black and can be seen as the central portion of each simulated interferogram. Densities falling within the seventh and eighth density range are also shaded black to provide the outer fringe of the hot gas region. This division of densities is arbitrary, but

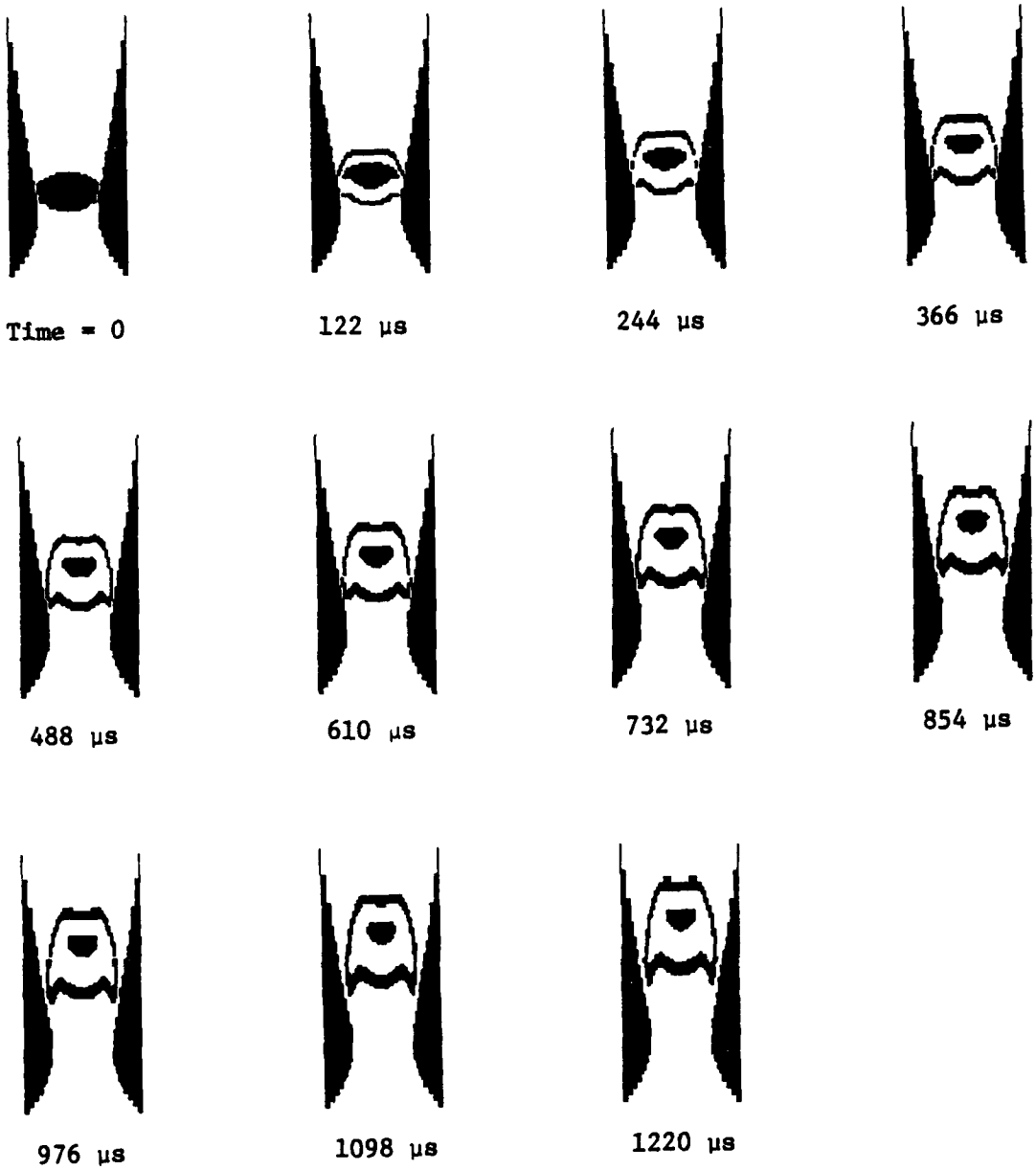

Figure 4.3 Simulated Interferograms for $\overline{U}$ = 5.5 m/s, θ = 5°
(500 K Initial Hot Gas Temperature)

serves to show the density variation in the interelectrode space for comparison with the first 11 interferograms of Figure 4.2.

As can be seen, the trends in the density variation compare rather favorably with the actual interferograms. The actual interferograms show some asymmetry near the electrodes, believed due to one electrode being hotter than the other. Both the experimentally obtained and the simulated interferograms show the effects of the hydrodynamic boundary layers retarding the flushing process near the electrodes.

To determine the effect of the value assumed for the initial temperature of the hot gas region, a second run was made with an assumed temperature of 700 K. The results are shown in Figure 4.4. A comparison of this figure with Figure 4.3 shows very little difference. The hot gas region for the case of the higher initial temperature accelerates slightly faster as it should since the density of the region is lower.

Although more work remains to be done to perfect the model, it is believed that the results presented here demonstrate the feasibility of such a model being used to predict the performance of gas blown switches. As was mentioned in the first section of this report, once gas density can be predicted, what remains to be done is to include a breakdown model for nonuniform density fields, so that the probability of prefires can then be predicted.

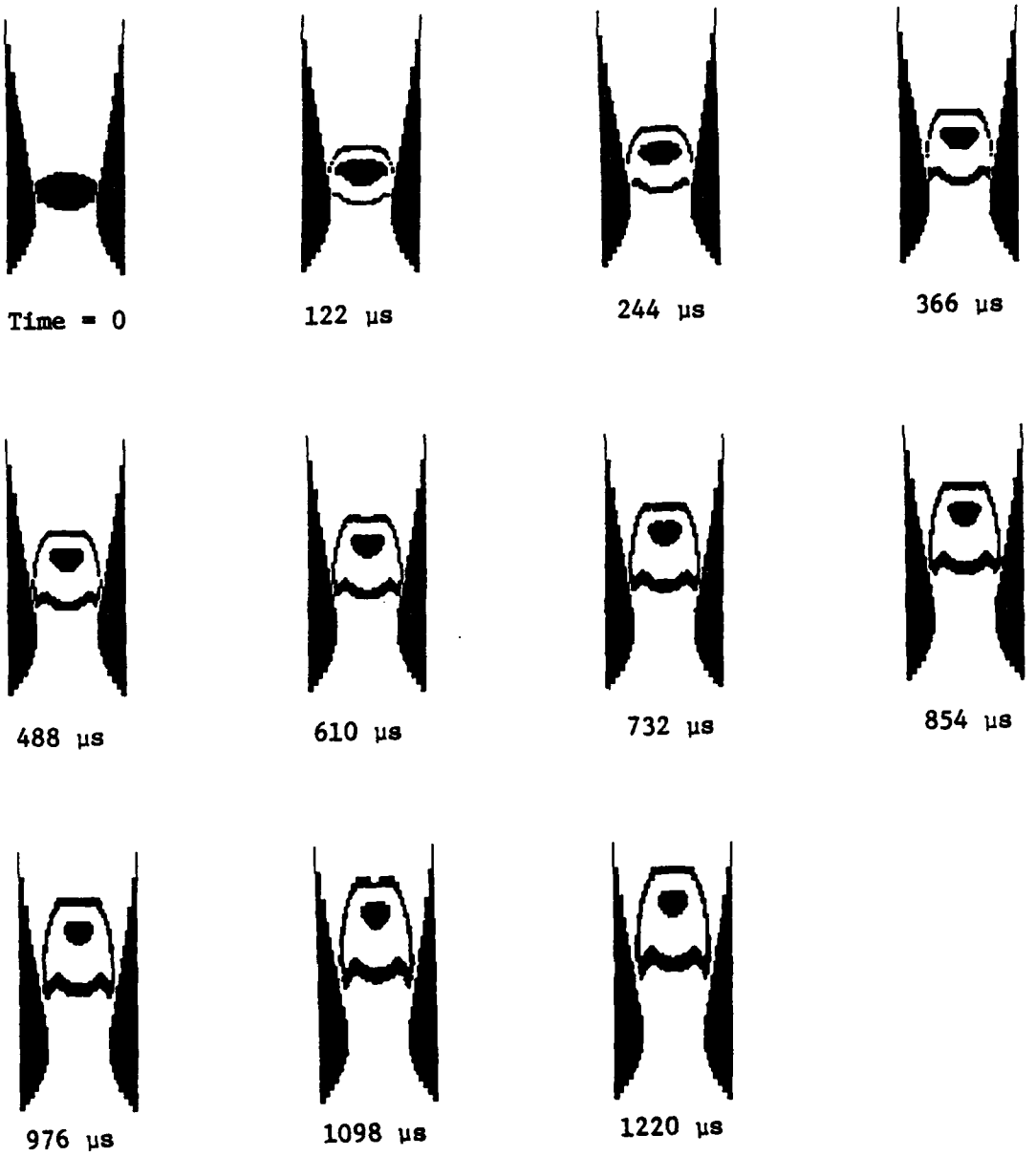

Figure 4.4 Simulated Interferograms for $\overline{U}$ = 5.5 m/s, θ = 5°
(700 K Initial Hot Gas Temperature)

V. WRITTEN PUBLICATIONS

The following papers were published as a result of the present study:

1. Pederson, R. J., and Carper, H. J., "Flow Visualization in a Gas-Blown Spark Gap," IEEE Conference Record of 1982 Fifteenth Power Modulator Symposium, pp. 105-109, June 1982.

2. Pederson, R. J., Borger, M. A., and Carper, H. J., "Effects of Flow Velocity and Electrode Divergence Angle on the Performance of a Repetitively Pulsed, Gas-Blown Spark Gap Switch," IEEE Conference Record of 1984 Sixteenth Power Modulator Symposium, pp. 48-53, June 1984.

VI. PROFESSIONAL PERSONNEL

The personnel who contributed to the work on the research project are listed below.

A. FACULTY

1. Herbert J. Carper, Jr., Associate Professor, Department of Mechanical Engineering, Principal Investigator.

2. Allen L. Goldman, Assistant Professor, Department of Mechanical Engineering, Co-Principal Investigator.

3. Ronald J. Pederson, Assistant Professor, Department of Mechanical Engineering, Co-Principal Investigator.

4. Timothy T. Maxwell, Associate Professor, Department of Mechanical Engineering, Co-Principal Investigator.

5. Preston F. Gott, Associate Professor, Department of Physics.

B. GRADUATE STUDENTS

1. Mark A. Borger, M. S. student in Mechanical Engineering. Thesis title: "The Effects of Electrode Divergence Angle and Mean Gap Velocity on the Peformance of Gas-Blown Spark Gap Switches, degree awarded August, 1984.

2. James R. Clark, M. S. student in Mechanical Engineering. Thesis title: "The Effects of Mass Flow Rate and Electrode Divergence Angle on the Performance of Gas-Blown Spark Gap Switches," degree awarded May, 1984.

3. Bradley L. Glass, M. S. student in Mechanical Engineering. Thesis title: "The Effects of Boundary Layer Development and Turbulence on the Performance of a Gas-Blown Spark Gap Switch," degree awarded December, 1984.

4. J. K. Shah, M. S. student in Mechanical Engineering. Thesis title: "Heat Conduction in a Three-Dimensional Body with Moving Boundaries," degree awarded December, 1983.

5. J. J. Sheu, M. S. student in Mechanical Engineering. Report title: "Visualization of the Flow in a Gas-Blown Spark Gap," degree awarded December, 1983.

6. H. H. Sung, M. S. student in Mechanical Engineering. Thesis title: "A Numerical Study for the Fluid Flow in a Spark Gap with Body-Fitted Coordinates," degree awarded May, 1983.

VII. INTERACTIONS

The following papers were presented at national conferences:

1. Pederson, R. J. and Carper, H. J., "Flow Visualization in a Gas-Blown Spark Gap," presented at the 1982 Fifteenth Power Modulator Symposium, Baltimore, Md., June 1982.

2. Pederson, R. J., Borger, M. A., and Carper, H. J., "Effects of Flow Velocity and Electrode Divergence Angle on the Performance of a Repetitively Pulsed, Gas-Blown Spark Gap Switch," presented at the 1984 Sixteenth Power Modulator Symposium, Arlington, Va., June 1984.

VIII. REFERENCES

1. Meek, J. M., and Craig, J. D., Electrical Breakdown of Gases, Wiley, Chichester, New York, 1978, p. 542.

2. Elderton, W. P., and Johnson, N. L., System of Frequency Curves, Cambridge University Press, London, England, pp. 51-58, pp. 67-70.

3. Metals Handbook, Vol. 1, Properties and Selection of Metals, 8th ed., American Society for Metals, 1961, p. 409.

4. Caretto, L. S., Gosman, A. D., Patankar, S. V., and Spalding, D. B., "Two Calculational Procedures for Steady, Three-Dimensional Flows with Recirculation," Heat Transfer Section Report No. HTS/72/5, Mechanical Engineering Department, Imperial College, London, England, 1972.

5. Patankar, S. V. and Spalding, D. B., "A Calculational Procedure for Heat, Mass and Momentum Transfer in Three-Dimensional Parabolic Flows," Int. J. of Heat and Mass Transfer, Vol. 15, pp. 1787-1806, 1972.

6. Patankar, S. V., Numerical Heat Transfer and Fluid Flow, Hemisphere Publishing Company, New York, 1980.

END

FILMED

1-86

DTIC